INTERNATIONAL JOURNAL OF
NUMERICAL ANALYSIS AND MODELING
Volume 23, Number 6, Pages 881–916

doi: 10.4208/ijnam2026-1036

UNCONDITIONAL ENERGY STABLE HYBRID IEQ-FEMS FOR THE CAHN-HILLIARD-NAVIER-STOKES EQUATIONS

YAOYAO CHEN, DONGQIAN LI, YIN YANG*, AND PEIMENG YIN

Abstract. We investigate two unconditionally energy stable invariant energy quadratization (IEQ) finite element methods (FEMs) [Chen et al. Numerical Algorithms, 99:1161-1202, 2025] for solving the Cahn-Hilliard-Navier-Stokes (CHNS) equations. The time discretization of these IEQ-FEMs is based on the first- and second-order backward differentiation methods. The auxiliary energy function introduced by the IEQ approach, modeling the square root of the nonlinear part of the energy, does not belong to the finite element space used for the spatial discretization. These methods offer distinct advantages. Consequently, we propose a new hybrid IEQ-FEM that combines the strengths of both schemes, offering computational efficiency and unconditional energy stability in the finite element space. We provide rigorous proofs of mass conservation and energy dissipation for the proposed IEQ-FEMs. Several numerical experiments are presented to validate the accuracy, efficiency, and solution properties of the proposed method.

Key words. IEQ-FEM, Stability, CHNS, BDF2, BDF1.

1. Introduction

This paper focuses on the development of unconditionally energy-stable finite element methods (FEMs) based on the invariant energy quadratization (IEQ) approach for solving the Cahn-Hilliard-Navier-Stokes (CHNS) problem [20, 27]

$$\partial_t \phi + \nabla \cdot (\mathbf{u}\phi) - \gamma \Delta w = 0 \qquad \text{in } \Omega \times (0,T], \tag{1a}$$

$$w + \lambda (\Delta \phi - f(\phi)) = 0 \qquad \text{in } \Omega \times (0,T], \tag{1b}$$

$$\partial_t \mathbf{u} - \mu \Delta \mathbf{u} + (\mathbf{u} \cdot \nabla)\mathbf{u} + \nabla p + \phi \nabla w = 0 \qquad \text{in } \Omega \times (0,T], \tag{1c}$$

$$\nabla \cdot \mathbf{u} = 0 \qquad \text{in } \Omega \times (0,T], \tag{1d}$$

$$\mathbf{u} = \mathbf{0}, \ \frac{\partial \phi}{\partial \nu} = 0, \ \frac{\partial w}{\partial \nu} = 0 \qquad \text{on } \partial\Omega \times (0,T], \tag{1e}$$

$$\mathbf{u}(\cdot,0) = \mathbf{u}_0, \ \phi(\cdot,0) = \phi_0 \qquad \text{in } \Omega, \tag{1f}$$

where $\Omega \subseteq \mathbb{R}^d (d = 2, 3)$ is a bounded domain, and ν represents the unit outward normal vector on the boundary $\partial\Omega$. Here, γ is a mobility constant related to the relaxation time scale, μ denotes the viscosity, and λ represents the magnitude of the mixing energy. $\mathbf{u}$ and p denote the velocity field and pressure, respectively. ϕ represents the phase field variable, where $\phi = \pm 1$ corresponds to two different fluids, and w is the chemical potential. The nonlinear term $f(\phi) = F'(\phi)$, where $F(\phi)$ represents the nonlinear bulk potential. The Dirichlet boundary conditions are imposed on the velocity field $\mathbf{u}$, while Neumann boundary conditions are applied to the phase field ϕ and potential w, as specified in (1e). One of well-known potentials is the double well potential

$$F(\phi) = \frac{1}{4\epsilon^2}(\phi^2 - 1)^2, \tag{2}$$

Received by the editors on December 8, 2024 and accepted on January 29, 2026.
2000 *Mathematics Subject Classification.* 65N12, 65N30, 35K55.
*Corresponding author.

where the parameter $\epsilon > 0$. The CHNS equations (1) is endowed with energy dissipation law

$$\frac{d}{dt}\mathcal{E}(\phi, \mathbf{u}) = -\int_{\Omega} \left(\mu|\nabla \mathbf{u}|^2 + \gamma|\nabla w|^2\right) d\mathbf{x} \leq 0, \tag{3}$$

with the total energy $\mathcal{E}(\phi, \mathbf{u}) = \int_{\Omega} \left(\frac{\lambda}{2}|\nabla\phi|^2 + \lambda F(\phi) + \frac{1}{2}|\mathbf{u}|^2\right) d\mathbf{x}$.

The physical phenomena captured by the two-phase flow model frequently occur in nature and various industrial processes [42]. Over the past few decades, the CHNS equations and its modifications have been applied to numerous situations, such as the solidification of liquid metal alloys [24], and the simulation of bubble dynamics [23].

There are many challenges in developing efficient and easy-to-implement numerical schemes for solving the phase-field CHNS equations. A key difficulty arises from the higher-order derivatives in the Cahn-Hilliard (CH) equations. One approach to address this is the use of the mixed methods, which reformulates the fourth-order phase field problem into a lower-order system, making it more amenable to numerical approximation. In recent years, several numerical schemes have been actively designed and applied to solve the CH equation or CHNS equations, including the FEMs [3, 6, 7], finite difference methods (FDMs) [40, 41], and spectral methods [4, 27, 33, 34, 38].

Another significant challenge is handling nonlinear terms, including the convection term $(\mathbf{u} \cdot \nabla)\mathbf{u}$, the coupling term $\phi\nabla w$ in the NS equation, and the convection term $\nabla \cdot (\mathbf{u}\phi)$ in the CH equation. For these terms, explicit-implicit methods are commonly used [34], and the projection method is applied to enforce a divergence-free velocity field [10, 25]. Additionally, efficiently managing the nonlinear term $f(\phi)$ in the CH equation poses another challenge. This term is often addressed using various techniques, such as the convex-splitting method [1, 13], the stabilization method [5, 27, 30], the IEQ approach [8, 18, 34, 35], the scalar auxiliary variable (SAV) approach [17, 26, 29, 41], and other related methods based on IEQ or SAV apparoach [3, 4, 21, 37, 38].

FEMs offer flexibility, accuracy, and the ability to handle complex geometries, nonlinearities, and multi-physics systems, making them widely used for solving the CHNS equations [3, 6, 31]. A straightforward idea for combining the IEQ approach with FEMs is to discretize the auxiliary variable introduced by IEQ directly within the finite element space. However, this leads to a scheme that is computationally expensive due to the need to invert the mass matrix [8]. The choice of function space for the auxiliary variable plays a crucial role in both computational efficiency and, in some cases, the physical fidelity of the numerical solution. Comparative studies on various IEQ-FEM schemes for the CahnHilliard and AllenCahn equations were carried out in [8], identifying two efficient approaches. In the first approach, the intermediate function is constrained to the continuous function space $C^0(\Omega)$, which enables efficient computation. However, because the computed energy cannot be directly evaluated in $C^0(\Omega)$, it must be interpolated into the finite element space. This may result in non-monotonic energy decay and potentially nonphysical behavior, despite the method's efficiency. The second approach computes the intermediate function in $C^0(\Omega)$ and then projects it into the finite element space. This projection ensures that the discrete energy law is unconditionally satisfied, albeit at the expense of additional computational cost. Motivated by these two methods, we extend them to the CHNS system and propose a novel hybrid IEQ-FEM

scheme that combines their strengthsachieving both computational efficiency and unconditional energy stability.

Solving the CHNS equations using the IEQ approach within the finite element method framework has not been thoroughly explored in the literature. In this work, we study several IEQ-FEMs for solving the CHNS equations. Specifically, we introduce two initial types of IEQ-FEMs, where the intermediate function is either in the combination of the polynomial space and the continuous function space, or only continuous function space. In the method where the intermediate function is in the combination of the polynomial space and the continuous function space, the function is first computed in the continuous function space $C^0(\Omega)$ and then projected onto the finite element space. This approach ensures that the numerical solutions are unconditionally energy-stable. The second method situates the intermediate function directly in the continuous function space $C^0(\Omega)$ rather than the finite element space. Since the intermediate function does not lie in the finite element space, the computed energy cannot be exactly evaluated in $C^0(\Omega)$ and must instead be interpolated within the finite element space. However, due to interpolation errors, the computed energy may not consistently exhibit decay, potentially leading to nonphysical solutions [8]. Nonetheless, conditional energy decay in finite element space can still be achieved.

Building on these, we propose a hybrid IEQ-FEM that begins with the IEQ-FEM with the intermediate function in the continuous function space. If the computed energy fails to exhibit dissipation, the scheme switches to the IEQ-FEM with projection onto the finite element space. This hybrid IEQ-FEM combines the advantages of both earlier methods: computational efficiency and unconditional energy stability in finite element space. Additionally, the phase field and velocity variables are approximated using piecewise quadratic finite elements, while the pressure variable is approximated by using piecewise linear finite elements. For time discretization, we apply first-order and second-order backward differentiation methods.

The rest of the paper is organized as follows. In Section 2, we first introduce the semi-discrete FEM for the CHNS equations, followed by an equivalent PDE system reformulated using the IEQ approach. In Section 3, we construct first- and second-order fully discrete IEQ-FEM schemes for the CHNS equations with an intermediate function in different function spaces. We rigorously prove the existence and uniqueness of the numerical solutions, along with the energy dissipation property. In Section 4, we present several numerical examples to demonstrate the effectiveness of the proposed schemes in solving the CHNS equations.

2. IEQ-FEMs for the CHNS Equations

In this section, we present the IEQ-FEMs for the CHNS equations (1). We begin by introducing the notations that will be used throughout the paper. Let $\alpha = (\alpha_1, \ldots, \alpha_d) \in \mathbb{Z}^d_{\geq 0}$ be a multi-index with $\partial^\alpha := \partial_1^{\alpha_1} \cdots \partial_{x_d}^{\alpha_d}$ and $|\alpha| := \sum_{i=1}^d \alpha_i$. The Sobolev space $H^m(\Omega)$, $m \geq 0$, consists of functions whose derivatives, corresponding to the multi-index α, are square integrable. Denote by $H_0^1(\Omega) \subset H^1(\Omega)$ the subspace consisting of functions with zero trace on the boundary $\partial\Omega$. Let $L^2(\Omega) := H^0(\Omega)$, and let $L_0^2(\Omega)$ be the subset of $L^2(\Omega)$ consisting of functions with zero average. For $s \geq 0$, $(H^s(\Omega))^d$ represents the vector space, such that $\mathbf{v} = (v_1, \ldots, v_d)^\top \in (H^s(\Omega))^d$ represents $v_i \in H^s(\Omega)$, $i = 1, \ldots, d$, where $\top$ is the transposition of a matrix or a vector.

Let $\mathcal{T}_h$ be a regular shape partition of Ω, with each $K \in \mathcal{T}_h$ being a quasi-uniform element in the finite element mesh $\mathcal{T}_h$. The diameter of each element K is denoted

by $h := \max\{h_K | h_K = \mathrm{diam}(K), K \in \mathcal{T}_h\}$. Define Y_h as a finite dimensional subspace of $H^1(\Omega)$, and $\mathbf{X}_h \times M_h \subset (H_0^1(\Omega))^d \times L_0^2(\Omega)$ as a pair of mixed finite element spaces, which satisfies the following *inf-sup* condition:

$$\inf_{q \in M_h} \sup_{\boldsymbol{v} \in \mathbf{X}_h} \frac{\left(\mathbf{B}^\top q, \boldsymbol{v}\right)}{\|\boldsymbol{v}\|_{H^1(\Omega)} \|q\|_{L^2(\Omega)}} \geq \beta_*, \tag{4}$$

where $\beta_* > 0$ is a constant, and the operator $\mathbf{B}^\top : M_h \to \mathbf{X}_h$ is the transpose of the discrete divergence operator $\mathbf{B} : \mathbf{X}_h \to M_h$. For every pair $(\boldsymbol{v}, \Phi) \in \mathbf{X}_h \times M_h$, it holds

$$(\mathbf{B}\boldsymbol{v}, \Phi) = (\boldsymbol{v}, \mathbf{B}^\top \Phi) = -(\nabla \cdot \boldsymbol{v}, \Phi).$$

Let $\mathbf{V}_h$ be a finite-dimensional subspace of $(L^2(\Omega))^d$. We assume either that $\mathbf{V}_h$ is conformal in $H_0^{\mathrm{div}}(\Omega)$ or that M_h is conformal in $H^1(\Omega)$. In this work, following [2, 11], we choose the finite element spaces as

$$\begin{aligned}
\mathbf{X}_h &= \mathbf{V}_h = \left\{ \mathbf{v}_h \in \left(C^0\left(\bar{\Omega}\right)\right)^d \cap \left(H_0^1(\Omega)\right)^d ; \mathbf{v}_h|_K \in \left(P_2(K)\right)^d \right\}, \\
M_h &= \left\{ \phi_h \in C^0(\bar{\Omega}) \cap L_0^2(\Omega); \phi_h|_K \in P_1(K) \right\}, \\
Y_h &= \left\{ \psi \in C^0\left(\bar{\Omega}\right); \psi_h|_K \in P_2(K) \right\}.
\end{aligned}$$

2.1. The semi-discrete FEM for the CHNS equations. The semi-discrete finite element scheme for the CHNS equations (1) is to find $(\phi_h, w_h, \mathbf{u}_h, p_h) \in Y_h \times Y_h \times \mathbf{X}_h \times M_h$ such that

$$(\partial_t \phi_h, \varphi) - (\mathbf{u}_h \phi_h, \nabla \varphi) - \gamma (\nabla w_h, \nabla \varphi) = 0, \ \forall \varphi \in Y_h, \tag{5a}$$

$$(w_h, \psi) - \lambda (\nabla \phi_h, \nabla \psi) - \lambda (f(\phi_h), \psi) = 0, \ \forall \psi \in Y_h, \tag{5b}$$

(5c)

$$(\partial_t \mathbf{u}_h, \mathbf{v}) + \mu (\nabla \mathbf{u}_h, \nabla \mathbf{v}) + ((\mathbf{u}_h \cdot \nabla) \mathbf{u}_h, \mathbf{v}) + (\nabla p_h, \mathbf{v}) + (\phi_h \nabla w_h, \mathbf{v}) = 0, \ \forall \mathbf{v} \in \mathbf{X}_h,$$

$$(\nabla \cdot \mathbf{u}_h, q) = 0, \ \forall q \in M_h. \tag{5d}$$

Here and in what follows, we denote by Π and $\mathbf{\Pi}$ the L^2 projection operators for scalar-valued and vector-valued functions, respectively. For any $\phi \in L^2(\Omega)$ and $\mathbf{u} \in (L^2(\Omega))^d$, the projections $\Pi\phi \in Y_h$ and $\mathbf{\Pi u} \in \mathbf{X}_h$ are defined by

$$\int_\Omega (\Pi\phi(x) - \phi(x)) \varphi \, d\mathbf{x} = 0, \quad \forall \varphi \in Y_h, \tag{6a}$$

$$\int_\Omega (\mathbf{\Pi u}(x) - \mathbf{u}(x)) \cdot \mathbf{v} \, d\mathbf{x} = 0, \quad \forall \mathbf{v} \in \mathbf{X}_h. \tag{6b}$$

The initial conditions for the semi-discrete finite element scheme (5) are given by

$$\mathbf{u}_h(\cdot, 0) = \mathbf{\Pi u}_0, \ \phi_h(\cdot, 0) = \Pi\phi_0. \tag{7}$$

We introduce the discrete free energy

$$\mathcal{E}(\phi_h, \mathbf{u}_h) = \int_\Omega \left(\frac{1}{2} |\mathbf{u}_h|^2 + \frac{\lambda}{2} |\nabla \phi_h|^2 + \lambda F(\phi_h) \right) d\mathbf{x}. \tag{8}$$

Then the following results hold.

Lemma 2.1. *The semi-discrete finite element scheme* (5) *conserves the total mass*

$$\frac{d}{dt} \int_\Omega \phi_h d\mathbf{x} = 0, \tag{9}$$

and the solution satisfies the energy dissipation law

$$\frac{d}{dt} \mathcal{E}(\phi_h, \mathbf{u}_h) = -\int_\Omega \left(\mu |\nabla \mathbf{u}_h|^2 + \gamma |\nabla w_h|^2 \right) d\mathbf{x} \leq 0. \tag{10}$$

2.2. The IEQ reformulation. Note that the potential $F(\phi_h)$ is uniformly bounded from below. The IEQ approach [32] transforms $F(\phi_h)$ into a quadratic form through an intermediate function

$$U = \sqrt{F(\phi_h) + B},$$

where B is a constant to ensure $F(\phi_h) + B > 0$. Consequently, the free energy (8) becomes

$$\mathcal{E}(\phi_h, \mathbf{u}_h, U) = \int_\Omega \left(\frac{1}{2}|\mathbf{u}_h|^2 + \frac{\lambda}{2}|\nabla \phi_h|^2 + \lambda U^2 \right) d\mathbf{x} - \lambda B|\Omega|. \tag{11}$$

By using the intermediate function U, the nonlinear term $F'(\phi_h)$ is substituted by

$$F'(\phi_h) = H(\phi_h) U,$$

where

$$H(\nu) = \frac{F'(\nu)}{\sqrt{F(\nu) + B}}.$$

The update of U is governed by

$$\partial_t U = \frac{1}{2} H(\phi_h) \partial_t \phi_h, \tag{12}$$

which is an ordinary differential equation for U, subject to the initial data

$$U(x, 0) = \sqrt{F(\phi_0(x)) + B}. \tag{13}$$

With the IEQ approach, the semi-discrete finite element scheme (5) can be reformulated as the following semi-discrete IEQ-FEM scheme

$$(\partial_t \phi_h, \varphi) - (\mathbf{u}_h \phi_h, \nabla \varphi) - \gamma (\nabla w_h, \nabla \varphi) = 0, \quad \forall \varphi \in Y_h, \tag{14a}$$

$$(w_h, \psi) - \lambda (\nabla \phi_h, \nabla \psi) - \lambda (H(\phi_h) U, \psi) = 0, \quad \forall \psi \in Y_h, \tag{14b}$$

(14c)

$$(\partial_t \mathbf{u}_h, \mathbf{v}) + \mu (\nabla \mathbf{u}_h, \nabla \mathbf{v}) + ((\mathbf{u}_h \cdot \nabla) \mathbf{u}_h, \mathbf{v}) + (\nabla p_h, \mathbf{v}) + (\phi_h \nabla w_h, \mathbf{v}) = 0, \quad \forall \mathbf{v} \in \mathbf{X}_h,$$

$$(\nabla \cdot \mathbf{u}_h, q) = 0, \quad \forall q \in M_h, \tag{14d}$$

$$\partial_t U = \frac{1}{2} H(\phi_h) \partial_t \phi_h. \tag{14e}$$

Then the following results hold.

Lemma 2.2. *The semi-discrete IEQ-FEM scheme* (14) *conserves the total mass*

$$\frac{d}{dt} \int_\Omega \phi_h d\mathbf{x} = 0, \tag{15}$$

and the solution satisfies the energy dissipation law

$$\frac{d}{dt} \mathcal{E}(\phi_h, \mathbf{u}_h, U) = -\int_\Omega \left(\mu |\nabla \mathbf{u}_h|^2 + \gamma |\nabla w_h|^2 \right) d\mathbf{x} \leq 0. \tag{16}$$

Proof. Choosing $\varphi = 1$ in (14a) gives the total mass conservation (15). From (14e), it follows

$$(H(\phi_h) U, \partial_t \phi_h) = (U, H(\phi_h) \partial_t \phi_h) = 2(U, \partial_t U) = \partial_t \|U\|^2. \tag{17}$$

By setting $\varphi = -w_h$ in (14a), $\psi = \partial_t \phi_h$ in (14b), and $\mathbf{v} = \mathbf{u}_h$ in (14c), the summation of (14a), (14b), and (14c) together with (17) yields (16). □

3. Fully discrete schemes

The main purpose of this section is to present the IEQ-FEM fully discrete schemes, where the spatial discretization is based on the finite element method, and the first- and second-order backward differentiation (BDF1 and BDF2 for short) are applied for the temporal discretization.

We consider a partition $0 = t_0 < t_1 < \cdots < t_N = T$ of $[0, T]$, the $(n+1)$-th subinterval is defined as $I_{n+1} := (t_n, t_{n+1}]$, and the corresponding time step $\tau_{n+1} := t_{n+1} - t_n, n = 0, \ldots, N-1$. For simplicity, we assume the time step $\tau_n = \tau > 0$ is a constant. For any given (vector) function $v(x,t)$ and $n \geq 0$, we denote $v^n := v(x, t_n)$ or v_h^n the approximation of $v(x,t)$ at t_n.

3.1. first-order fully discrete schemes. In this section, we first introduce two types of first-order fully discrete IEQ-FEM schemes for the CHNS equations, where the intermediate function U in the semi-discrete IEQ-FEM scheme (14) is positioned in either the polynomial space or the continuous function space. We then propose a new method that combines both of these schemes.

3.1.1. P-BDF1 scheme. To design a first-order, fully decoupled, and fully discrete IEQ-FEM scheme, we apply a splitting strategy to the CHNS problem (1). Following the idea in [12], the pressure p in (1c) can be computed separately from the velocity field $\mathbf{u}$. Assume that w, and ϕ has been computed. First, if an approximation $p(=\tilde{p})$ of pressure is available, we can directly solve for $\mathbf{u}$ from

$$\partial_t \mathbf{u} - \mu \Delta \mathbf{u} + (\mathbf{u} \cdot \nabla)\, \mathbf{u} + \nabla \tilde{p} + \phi \nabla w = 0. \tag{18}$$

Note that $\mathbf{u}$ from (18) is not necessarily divergence-free. Second, if $\mathbf{u}$ is known, the pressure p can be recovered by testing (1c) with ∇q. Using $(\partial_t \mathbf{u}, \nabla q) = -(\nabla \cdot \partial_t \mathbf{u}, q) = 0$ yields

$$(\nabla p, \nabla q) = \left(\mu \Delta \mathbf{u} - (\mathbf{u} \cdot \nabla)\, \mathbf{u} - \phi \nabla w, \nabla q\right), \quad \forall q \in H^1(\Omega), \tag{19}$$

which corresponds to the relation

$$\nabla \bar{p} := \mu \Delta \mathbf{u} - (\mathbf{u} \cdot \nabla)\, \mathbf{u} - \phi \nabla w. \tag{20}$$

Observe that the true pressure p in (1c) satisfies

$$\nabla p = -\partial_t \mathbf{u} + \mu \Delta \mathbf{u} - (\mathbf{u} \cdot \nabla)\, \mathbf{u} - \phi \nabla w. \tag{21}$$

Subtracting (20) from (21) yields

$$\partial_t \mathbf{u} + \nabla (p - \bar{p}) = 0, \tag{22}$$

so enforcing the incompressible condition (1d) on (22) provides a corrected (divergence-free) pair $(\mathbf{u}, p)$ that serves as an alternative solution to (1c).

Hence, the solution $(\mathbf{u}, p)$ at t_{n+1} to the NS equation (1c) can be approximated from the following first-order splitting scheme:

$$\partial_t \tilde{\mathbf{u}} - \mu \Delta \tilde{\mathbf{u}} + (\tilde{\mathbf{u}} \cdot \nabla)\, \tilde{\mathbf{u}} + \nabla p^n + \phi \nabla w = 0, \quad \tilde{\mathbf{u}}(x, t_n) = \mathbf{u}^n, \tag{23a}$$

$$\partial_t \mathbf{u} + \nabla (p - p^n) = 0, \qquad \mathbf{u}(x, t_n) = \tilde{\mathbf{u}}(x, t_{n+1}). \tag{23b}$$

Here, we slightly abuse the notation $\mathbf{u}^n$ in (23a) and $\mathbf{u}(x, t_n)$ in (23b). Although they should be identical in meaning, $\mathbf{u}^n$ in (23a) denotes the velocity obtained from the previous time step, while $\mathbf{u}(x, t_n)$ in (23b) represents the initial condition of the current subproblem at time t_n. Here, the first substep (23a) advances an intermediate velocity $\tilde{\mathbf{u}}$ using the known pressure p^n, while the second substep (23b) updates the pressure and corrects the velocity field to enforce the incompressible condition

(1d). The intermediate velocity $\tilde{\mathbf{u}}$ is generally not divergence-free, whereas the corrected velocity $\mathbf{u}$ at t_{n+1} satisfies $\nabla \cdot \mathbf{u} = 0$.

The first-order fully discrete IEQ-FEM for (1) with (1c) split by (23) is now ready to present. We first project the intermediate function U^n onto the polynomial space Y_h. Given $(\phi_h^n, \mathbf{u}_h^n) \in Y_h \times \mathbf{V}_h$ and $U^n \in C^0(\Omega)$, the P-BDF1 scheme is to find $(\phi_h^{n+1}, w_h^{n+1}, \tilde{\mathbf{u}}_h^{n+1}, \mathbf{u}_h^{n+1}, p_h^{n+1}) \in Y_h \times Y_h \times \mathbf{X}_h \times \mathbf{V}_h \times M_h$ and $U^{n+1} \in C^0(\Omega)$, $\hat{\mathbf{u}}^{n+1} \in (L^2(\Omega))^d$ such that

$$\left(\frac{\phi_h^{n+1} - \phi_h^n}{\tau}, \varphi_h\right) - \left(\hat{\mathbf{u}}^{n+1}\phi_h^n, \nabla\varphi_h\right) + \gamma a\left(w_h^{n+1}, \varphi_h\right) = 0, \qquad \forall \varphi_h \in Y_h, \tag{24a}$$

$$\left(w_h^{n+1}, \psi_h\right) - \lambda a\left(\phi_h^{n+1}, \psi_h\right) - \lambda\left(H\left(\phi_h^n\right) U^{n+1}, \psi_h\right) = 0, \qquad \forall \psi_h \in Y_h, \tag{24b}$$

$$\hat{\mathbf{u}}^{n+1} = \mathbf{u}_h^n - \tau\phi_h^n \nabla w_h^{n+1}, \tag{24c}$$

$$\left(U_h^n, \mu_h\right) = \left(U^n, \mu_h\right), \qquad \forall \mu_h \in Y_h, \tag{24d}$$

$$U^{n+1} = U_h^n + \frac{1}{2} H\left(\phi_h^n\right)\left(\phi_h^{n+1} - \phi_h^n\right), \tag{24e}$$

$$\begin{aligned}\left(\frac{\tilde{\mathbf{u}}_h^{n+1} - \mathbf{u}_h^n}{\tau}, \mathbf{v}_h\right) + \mu\tilde{a}\left(\tilde{\mathbf{u}}_h^{n+1}, \mathbf{v}_h\right) + b\left(\mathbf{u}_h^n, \tilde{\mathbf{u}}_h^{n+1}, \mathbf{v}_h\right) - \left(p_h^n, \nabla \cdot \mathbf{v}_h\right) \\ + \left(\phi_h^n \nabla w_h^{n+1}, \mathbf{v}_h\right) = 0, \qquad \forall \mathbf{v}_h \in \mathbf{X}_h,\end{aligned} \tag{25}$$

and

$$\begin{aligned}\left(\frac{\mathbf{u}_h^{n+1} - \tilde{\mathbf{u}}_h^{n+1}}{\tau}, \chi_h\right) - \left(\left(p_h^{n+1} - p_h^n\right), \nabla \cdot \chi_h\right) = 0, \qquad \forall \chi_h \in \mathbf{V}_h, \\ \left(\nabla \cdot \mathbf{u}_h^{n+1}, q_h\right) = 0, \qquad \forall q_h \in M_h,\end{aligned} \tag{26}$$

where

$$\begin{aligned} a(w, \phi) &= (\nabla w, \nabla \phi), && \forall w, \phi \in H^1(\Omega), \\ \tilde{a}(\mathbf{u}, \mathbf{v}) &= (\nabla \mathbf{u}, \nabla \mathbf{v}), && \forall \mathbf{u}, \mathbf{v} \in (H^1(\Omega))^d, \\ b(\mathbf{u}, \mathbf{v}, \mathbf{w}) &= ((\mathbf{u} \cdot \nabla)\mathbf{v}, \mathbf{w}) + \frac{1}{2}((\nabla \cdot \mathbf{u})\mathbf{v}, \mathbf{w}), && \forall \mathbf{u}, \mathbf{v}, \mathbf{w} \in (H^1(\Omega))^d. \end{aligned} \tag{27}$$

The initial data $(\phi_h^0, \mathbf{u}_h^0, U^0)$ is given by (7) and (13).

Remark 3.1. In the P-BDF1 scheme, the projection step (24d) represents an L^2 projection, while (26) corresponds to the projection step used in the Navier-Stokes equations. The latter realizes the identity $\mathbf{u}_h^{n+1} = P_H \tilde{\mathbf{u}}_h^{n+1}$, where the operator $P_H : \mathbf{X}_h \to \ker(\mathbf{B})$ [11]. To avoid ambiguity, we will distinguish these two types of projection by explicitly referencing their equation numbers throughout the remainder of this article.

Remark 3.2. For the P-BDF1 scheme (24)-(26), given $(\phi_h^n, w_h^n, U^n, \mathbf{u}_h^n, p_h^n)$, we first compute U_h^n from the projection step in equation (24d). $\hat{\mathbf{u}}^{n+1} \in (L^2(\Omega))^d$ in (24a) is an intermediate function containing a stabilization term, and itself is not computed in the algorithm. $(\phi_h^{n+1}, w_h^{n+1})$ is obtained by solving the linear system formed by equations (24a) and (24b), with the substitutions from equations (24c) and (24e),

respectively

(28)
$$\left(\frac{\phi_h^{n+1}-\phi_h^n}{\tau},\varphi_h\right)-(\mathbf{u}_h^n\phi_h^n,\nabla\varphi_h)+\tau\left((\phi_h^n)^2\nabla w_h^{n+1},\nabla\varphi_h\right)+\gamma a\left(w_h^{n+1},\varphi_h\right)=0,$$

(29)
$$\left(w_h^{n+1},\psi_h\right)-\lambda a(\phi_h^{n+1},\psi_h)=\lambda\left(H(\phi_h^n)U_h^n,\psi_h\right)+\frac{1}{2}\lambda\left(H(\phi_h^n)^2(\phi_h^{n+1}-\phi_h^n),\psi_h\right),$$

where each term in (28)-(29) can be computed by using Gaussian quadrature, which is equivalent to the process of L^2 projection. Then, we update U^{n+1} from (24e). For the Navier-Stokes part, the intermediate velocity $\tilde{\mathbf{u}}_h^{n+1}$ is computed from (25), followed by the projection step (26) to obtain $(\mathbf{u}_h^{n+1},p_h^{n+1})$. All resulting subproblems are linear systems, which can be solved by appropriate linear solvers.

Remark 3.3. Although the original Cahn–Hilliard equation contains a fourth-order differential operator, we reduce its order by introducing an auxiliary variable w. This reformulation converts the fourth-order equation into a system of two coupled second-order equations, thereby avoiding the challenges of directly discretizing fourth-order terms and allowing the use of C^0 finite elements.

Remark 3.4. The proposed methods and their analysis are applicable to other boundary conditions, such as nonhomogeneous mixed Dirichlet-Neumann boundary conditions and the periodic boundary conditions [14, 38]. For the nonhomogeneous Neumann boundary condition, assume that the phase field variables ϕ and w satisfy $\frac{\partial\phi}{\partial\nu}=\phi_N$, $\frac{\partial w}{\partial\nu}=w_N$. Applying the integration-by-parts formula, we reformulate Eqs. (24a)-(24b) in the P-BDF1 scheme as follows

$$\begin{aligned}
&\left(\frac{\phi_h^{n+1}-\phi_h^n}{\tau},\varphi_h\right)-(\mathbf{u}_h^n\phi_h^n,\nabla\varphi_h)+\tau\left((\phi_h^n)^2\nabla w_h^{n+1},\nabla\varphi_h\right)\\
&\qquad+\gamma a\left(w_h^{n+1},\varphi_h\right)-\gamma(w_N^{n+1},\varphi_h)_{\partial\Omega}=0,\\
&\left(w_h^{n+1},\psi_h\right)-\lambda a(\phi_h^{n+1},\psi_h)+\lambda(\phi_N^{n+1},\psi_h)_{\partial\Omega}=\lambda\left(H(\phi_h^n)U_h^n,\psi_h\right)\\
&\qquad+\frac{1}{2}\lambda\left(H(\phi_h^n)^2(\phi_h^{n+1}-\phi_h^n),\psi_h\right),
\end{aligned}$$

where $(p,q)_{\partial\Omega}=\int_{\partial\Omega}pqds$. Similarly, the proposed methods can be adapted to handle nonhomogeneous Dirichlet boundary conditions and periodic boundary conditions by modifying the finite element spaces and enforcing the prescribed boundary values appropriately. It is worth noting that the types of the boundary condition does not affect the ODE (12) or its discrete forms, as they depend only on the initial data.

Lemma 3.5. [6] *The bilinear form* $b\left(\mathbf{u}_h^n,\cdot,\cdot\right)$ *in the fully discrete scheme* (24)-(26) *is skew symmetric. Especially, it holds that*

$$b\left(\mathbf{u}_h^n,\tilde{\mathbf{u}}_h^{n+1},\tilde{\mathbf{u}}_h^{n+1}\right)=0,\qquad\forall\tilde{\mathbf{u}}_h^{n+1}\in\mathbf{X}_h. \tag{30}$$

Lemma 3.6. *The solution of* (24)-(26) *conserves the total mass*

$$\int_\Omega\phi_h^{n+1}d\mathbf{x}=\int_\Omega\phi_h^0d\mathbf{x}. \tag{31}$$

Proof. Taking $\varphi_h=1$ in (24a) yields the conservation of total mass. □

For scheme (24)-(26), we establish the following result.

Theorem 3.7. *The P-BDF1 scheme* (24)-(26) *admits a unique solution set*

$$(\phi_h^{n+1}, w_h^{n+1}, \mathbf{u}_h^{n+1}, p_h^{n+1}) \in Y_h \times Y_h \times \mathbf{V}_h \times M_h,$$

and $U^{n+1} \in C^0(\Omega)$.

Proof. Since equations (24)(26) constitute a finite-dimensional linear system, the existence of a solution is equivalent to its uniqueness. Now, assume that the linear system (24)(26) has two solutions, and denote their difference at t^{n+1} by $(\delta\phi_h^{n+1}, \delta w_h^{n+1}, \delta\hat{\mathbf{u}}_h^{n+1}, \delta\tilde{\mathbf{u}}_h^{n+1}, \delta\mathbf{u}_h^{n+1}, \delta p_h^{n+1})$, then it follows

$$\frac{1}{\tau}\left(\delta\phi_h^{n+1}, \varphi_h\right) - \left(\delta\hat{\mathbf{u}}_h^{n+1}\phi_h^n, \nabla\varphi_h\right) + \gamma a\left(\delta w_h^{n+1}, \varphi_h\right) = 0, \qquad \forall\varphi_h \in Y_h, \tag{32a}$$

$$\left(\delta w_h^{n+1}, \psi_h\right) - \lambda a\left(\delta\phi_h^{n+1}, \psi_h\right) - \frac{\lambda}{2}\left(H^2\left(\phi_h^n\right)\delta\phi_h^{n+1}, \psi_h\right) = 0, \qquad \forall\psi_h \in Y_h, \tag{32b}$$

$$\delta\hat{\mathbf{u}}^{n+1} = -\tau\phi_h^n\nabla\delta w_h^{n+1}. \tag{32c}$$

Taking $\varphi_h = \tau\delta w_h^{n+1}$, $\psi_h = \delta\phi_h^{n+1}$ in (32a) and (32b), respectively, multiplying both sides of equation (32c) by $\delta\hat{\mathbf{u}}^{n+1}$, and summing them up yields

$$\tau\gamma|\delta w_h^{n+1}|^2_{H^1(\Omega)} + \lambda|\delta\phi_h^{n+1}|^2_{H^1(\Omega)} + \frac{\lambda}{2}\left\|H(\phi_h^n)\delta\phi_h^{n+1}\right\|^2 + \left\|\delta\hat{\mathbf{u}}^{n+1}\right\|^2 = 0, \tag{33}$$

which implies $\delta\hat{\mathbf{u}}^{n+1} = 0$ and $\delta w_h^{n+1} = \delta\phi_h^{n+1} =$ Constant. Then, plugging them into (32a) and (32b) leads to $\left(\delta\phi_h^{n+1}, \varphi_h\right) = \left(\delta w_h^{n+1}, \psi_h\right) = 0$, $\forall\varphi_h$, $\psi_h \in Y_h$, which implies $\delta w_h^{n+1} = \delta\phi_h^{n+1} = 0$.

We note that U^{n+1} is determined by the known variables ϕ_h^n, U_h^n and the unique solution ϕ_h^{n+1}, and is therefore unique. $\delta\tilde{\mathbf{u}}_h^{n+1}$ satisfies

$$\frac{1}{\tau}\left(\delta\tilde{\mathbf{u}}_h^{n+1}, \mathbf{v}_h\right) + \mu\tilde{a}\left(\delta\tilde{\mathbf{u}}_h^{n+1}, \mathbf{v}_h\right) + b\left(\mathbf{u}_h^n, \delta\tilde{\mathbf{u}}_h^{n+1}, \mathbf{v}_h\right) = 0, \qquad \forall\mathbf{v}_h \in \mathbf{X}_h. \tag{34}$$

Taking $\mathbf{v}_h = \delta\tilde{\mathbf{u}}_h^{n+1}$ and using Lemma 3.5, we obtain

$$\left\|\delta\tilde{\mathbf{u}}_h^{n+1}\right\|^2 = 0,$$

namely,

$$\delta\tilde{\mathbf{u}}_h^{n+1} = 0.$$

Finally, the variable $\delta\mathbf{u}_h^{n+1}$ satisfies the following equations:

$$\begin{aligned} \left(\delta\mathbf{u}_h^{n+1}, \chi_h\right) - \left((\delta p_h^{n+1}), \nabla\cdot\chi_h\right) &= 0, \qquad \forall\chi_h \in \mathbf{V}_h, \\ \left(\nabla\cdot(\delta\mathbf{u}_h^{n+1}), q_h\right) &= 0, \qquad \forall q_h \in M_h. \end{aligned} \tag{35}$$

Taking $\chi_h = \delta\mathbf{u}_h^{n+1}$ and $q_h = \delta p_h^{n+1}$ in (35) yield $\left\|\delta\tilde{\mathbf{u}}_h^{n+1}\right\|^2 = 0$, namely, $\delta\tilde{\mathbf{u}}_h^{n+1} = 0$, which together with the first equation in (35) and inf-sup condition (4) further implies $\nabla(\delta p_h^{n+1}) = 0$. □

Theorem 3.8. *For the CHNS equations* (1)*, the P-BDF1 scheme* (24)-(26) *is unconditionally energy stable and satisfies the following modified discrete energy law:*

$$\begin{aligned} E\left(\phi_h^{n+1}, \mathbf{u}_h^{n+1}, U_h^{n+1}, p_h^{n+1}\right) &\le E\left(\phi_h^{n+1}, \mathbf{u}_h^{n+1}, U^{n+1}, p_h^{n+1}\right) \\ &= E\left(\phi_h^n, \mathbf{u}_h^n, U_h^n, p_h^n\right) - \tau\gamma\left\|\nabla w_h^{n+1}\right\|^2 - \tau\mu\left\|\nabla\tilde{\mathbf{u}}_h^{n+1}\right\|^2 \\ &\quad - \frac{\lambda}{2}\left\|\nabla\left(\phi_h^{n+1} - \phi_h^n\right)\right\|^2 - \lambda\left\|U^{n+1} - U_h^n\right\|^2 \\ &\quad - \frac{1}{2}\left\|\hat{\mathbf{u}}^{n+1} - \mathbf{u}_h^n\right\|^2 - \frac{1}{2}\left\|\tilde{\mathbf{u}}_h^{n+1} - \hat{\mathbf{u}}^{n+1}\right\|^2, \end{aligned} \tag{36}$$

where

$$E\left(\phi_h^{n+1},\mathbf{u}_h^{n+1},U_h^{n+1},p_h^{n+1}\right)=\mathcal{E}\left(\phi_h^{n+1},\mathbf{u}_h^{n+1},U_h^{n+1}\right)+\frac{\tau^2}{2}\left\|\nabla p_h^{n+1}\right\|,$$

and $\mathcal{E}\left(\phi_h^{n+1},\mathbf{u}_h^{n+1},U^{n+1}\right)$ *is defined in equation* (11).

Proof. Step 1: Taking $\varphi_h=\tau w_h^{n+1}\in Y_h$ in (24a), $\psi_h=-\left(\phi_h^{n+1}-\phi_h^n\right)\in Y_h$ in (24b), $\mathbf{v}_h=\tau\tilde{\mathbf{u}}_h^{n+1}\in\mathbf{X}_h$ in (25) give

$$\begin{aligned}&\left(\phi_h^{n+1}-\phi_h^n,w_h^{n+1}\right)+\tau\left(\nabla\cdot\left(\hat{\mathbf{u}}^{n+1}\phi_h^n\right),w_h^{n+1}\right)+\tau\gamma a\left(w_h^{n+1},w_h^{n+1}\right)=0,\\&-\left(w_h^{n+1},\phi_h^{n+1}-\phi_h^n\right)+\lambda a\left(\phi_h^{n+1},\phi_h^{n+1}-\phi_h^n\right)\\&+\lambda\left(H\left(\phi_h^n\right)U^{n+1},\phi_h^{n+1}-\phi_h^n\right)=0,\\&\left(\tilde{\mathbf{u}}_h^{n+1}-\mathbf{u}_h^n,\tilde{\mathbf{u}}_h^{n+1}\right)+\tau\mu\tilde{a}\left(\tilde{\mathbf{u}}_h^{n+1},\tilde{\mathbf{u}}_h^{n+1}\right)\\&-\tau\left(p_h^n,\nabla\cdot\tilde{\mathbf{u}}_h^{n+1}\right)+\tau\left(\phi_h^n\nabla w_h^{n+1},\tilde{\mathbf{u}}_h^{n+1}\right)=0.\end{aligned}\tag{37}$$

The summation of (37) yields

$$\begin{aligned}&\tau\left(\nabla\cdot\left(\hat{\mathbf{u}}^{n+1}\phi_h^n\right),w_h^{n+1}\right)+\tau\gamma\left\|\nabla w_h^{n+1}\right\|^2+\lambda a\left(\phi_h^{n+1},\phi_h^{n+1}-\phi_h^n\right)\\&+\lambda\left(H\left(\phi_h^n\right)U^{n+1},\phi_h^{n+1}-\phi_h^n\right)+\left(\tilde{\mathbf{u}}_h^{n+1}-\mathbf{u}_h^n,\tilde{\mathbf{u}}_h^{n+1}\right)\\&+\tau\mu\left\|\nabla\tilde{\mathbf{u}}_h^{n+1}\right\|^2-\tau\left(p_h^n,\nabla\cdot\tilde{\mathbf{u}}_h^{n+1}\right)+\tau\left(\phi_h^n\nabla w_h^{n+1},\tilde{\mathbf{u}}_h^{n+1}\right)=0.\end{aligned}\tag{38}$$

Upon regrouping, it follows

$$\begin{aligned}&-\tau\left(\hat{\mathbf{u}}^{n+1}\phi_h^n,\nabla w_h^{n+1}\right)+\tau\gamma\left\|\nabla w_h^{n+1}\right\|^2\\&+\tfrac{\lambda}{2}\left(\left\|\nabla\phi_h^{n+1}\right\|^2+\left\|\nabla\left(\phi_h^{n+1}-\phi_h^n\right)\right\|^2-\left\|\nabla\phi_h^n\right\|^2\right)\\&+\lambda\left(\left\|U^{n+1}\right\|^2+\left\|U^{n+1}-U_h^n\right\|^2-\left\|U_h^n\right\|^2\right)+\left(\tilde{\mathbf{u}}_h^{n+1}-\mathbf{u}_h^n,\tilde{\mathbf{u}}_h^{n+1}\right)\\&+\tau\mu\left\|\nabla\tilde{\mathbf{u}}_h^{n+1}\right\|^2-\tau\left(p_h^n,\nabla\cdot\tilde{\mathbf{u}}_h^{n+1}\right)+\tau\left(\phi_h^n\nabla w_h^{n+1},\tilde{\mathbf{u}}_h^{n+1}\right)=0.\end{aligned}\tag{39}$$

Step 2: Multiplying (24c) by $\tilde{\mathbf{u}}_h^{n+1}$ and $\hat{\mathbf{u}}^{n+1}$, respectively, gives

$$\left(\hat{\mathbf{u}}^{n+1},\tilde{\mathbf{u}}_h^{n+1}\right)=\left(\mathbf{u}_h^n,\tilde{\mathbf{u}}_h^{n+1}\right)-\tau\left(\phi_h^n\nabla w_h^{n+1},\tilde{\mathbf{u}}_h^{n+1}\right),\tag{40}$$

$$\left(\hat{\mathbf{u}}^{n+1},\hat{\mathbf{u}}^{n+1}\right)=\left(\mathbf{u}_h^n,\hat{\mathbf{u}}^{n+1}\right)-\tau\left(\phi_h^n\nabla w_h^{n+1},\hat{\mathbf{u}}^{n+1}\right).\tag{41}$$

Plugging (40) and (41) into (39) gives

$$\begin{aligned}&\left(\hat{\mathbf{u}}^{n+1}-\mathbf{u}_h^n,\hat{\mathbf{u}}^{n+1}\right)+\tau\gamma\left\|\nabla w_h^{n+1}\right\|^2\\&+\frac{\lambda}{2}\left(\left\|\nabla\phi_h^{n+1}\right\|^2+\left\|\nabla\left(\phi_h^{n+1}-\phi_h^n\right)\right\|^2-\left\|\nabla\phi_h^n\right\|^2\right)\\&+\lambda\left(\left\|U^{n+1}\right\|^2+\left\|U^{n+1}-U_h^n\right\|^2-\left\|U_h^n\right\|^2\right)+\left(\tilde{\mathbf{u}}_h^{n+1}-\mathbf{u}_h^n,\tilde{\mathbf{u}}_h^{n+1}\right)\\&+\tau\mu\left\|\nabla\tilde{\mathbf{u}}_h^{n+1}\right\|^2-\tau\left(p_h^n,\nabla\cdot\tilde{\mathbf{u}}_h^{n+1}\right)-\left(\hat{\mathbf{u}}^{n+1}-\mathbf{u}_h^n,\tilde{\mathbf{u}}_h^{n+1}\right)=0.\end{aligned}\tag{42}$$

Upon simplification, it follows

$$\begin{aligned}&\frac{1}{2}\left(\left\|\hat{\mathbf{u}}^{n+1}\right\|^2+\left\|\hat{\mathbf{u}}^{n+1}-\mathbf{u}_h^n\right\|^2-\left\|\mathbf{u}_h^n\right\|^2\right)\\&+\frac{\lambda}{2}\left(\left\|\nabla\phi_h^{n+1}\right\|^2+\left\|\nabla\left(\phi_h^{n+1}-\phi_h^n\right)\right\|^2-\left\|\nabla\phi_h^n\right\|^2\right)\\&+\tau\gamma\left\|\nabla w_h^{n+1}\right\|^2+\lambda\left(\left\|U^{n+1}\right\|^2+\left\|U^{n+1}-U_h^n\right\|^2-\left\|U_h^n\right\|^2\right)\\&+\frac{1}{2}\left(\left\|\tilde{\mathbf{u}}_h^{n+1}\right\|^2+\left\|\tilde{\mathbf{u}}_h^{n+1}-\hat{\mathbf{u}}^{n+1}\right\|^2-\left\|\hat{\mathbf{u}}^{n+1}\right\|^2\right)\\&+\tau\mu\left\|\nabla\tilde{\mathbf{u}}_h^{n+1}\right\|^2-\tau\left(p_h^n,\nabla\cdot\tilde{\mathbf{u}}_h^{n+1}\right)=0.\end{aligned}\tag{43}$$

Step 3: Let $\chi_h = \tau\nabla p_h^n,\ q_h = p_h^n$ in (26). Then the summation gives

$$-\left(\tilde{\mathbf{u}}_h^{n+1}, \nabla p_h^n\right) + \frac{\tau}{2}\left(\left\|\nabla p_h^{n+1}\right\|^2 - \left\|\nabla\left(p_h^{n+1} - p_h^n\right)\right\|^2 - \left\|\nabla p_h^n\right\|^2\right) = 0. \tag{44}$$

By plugging (44) into (43) to replace $-\tau\left(p_h^n, \nabla\cdot\tilde{\mathbf{u}}_h^{n+1}\right)$, it holds

$$\begin{aligned}
&\frac{1}{2}\left(\left\|\hat{\mathbf{u}}^{n+1}\right\|^2 + \left\|\hat{\mathbf{u}}^{n+1} - \mathbf{u}_h^n\right\|^2 - \left\|\mathbf{u}_h^n\right\|^2\right)\\
&+\frac{\lambda}{2}\left(\left\|\nabla\phi_h^{n+1}\right\|^2 + \left\|\nabla\left(\phi_h^{n+1} - \phi_h^n\right)\right\|^2 - \left\|\nabla\phi_h^n\right\|^2\right)\\
&+\tau\gamma\left\|\nabla w_h^{n+1}\right\|^2 + \lambda\left(\left\|U^{n+1}\right\|^2 + \left\|U^{n+1} - U_h^n\right\|^2 - \left\|U_h^n\right\|^2\right)\\
&+\frac{1}{2}\left(\left\|\tilde{\mathbf{u}}_h^{n+1}\right\|^2 + \left\|\tilde{\mathbf{u}}_h^{n+1} - \hat{\mathbf{u}}^{n+1}\right\|^2 - \left\|\hat{\mathbf{u}}^{n+1}\right\|^2\right) + \tau\mu\left\|\nabla\tilde{\mathbf{u}}_h^{n+1}\right\|^2\\
&+\frac{\tau^2}{2}\left(\left\|\nabla p_h^{n+1}\right\|^2 - \left\|\nabla\left(p_h^{n+1} - p_h^n\right)\right\|^2 - \left\|\nabla p_h^n\right\|^2\right) = 0.
\end{aligned} \tag{45}$$

Step 4: Further, taking χ_h as $\tau\left(\mathbf{u}_h^{n+1} + \tilde{\mathbf{u}}_h^{n+1}\right)$ and $\tau\nabla\left(p_h^{n+1} - p_h^n\right)$, respectively, and $q_h = p_h^{n+1} - p_h^n$ in (26), it gives

$$\begin{aligned}
&\left(\mathbf{u}_h^{n+1} - \tilde{\mathbf{u}}_h^{n+1}, \mathbf{u}_h^{n+1} + \tilde{\mathbf{u}}_h^{n+1}\right) + \tau\left(\nabla\left(p_h^{n+1} - p_h^n\right), \mathbf{u}_h^{n+1} + \tilde{\mathbf{u}}_h^{n+1}\right) = 0,\\
&\left(\mathbf{u}_h^{n+1} - \tilde{\mathbf{u}}_h^{n+1}, \nabla\left(p_h^{n+1} - p_h^n\right)\right) + \tau\left(\nabla\left(p_h^{n+1} - p_h^n\right), \nabla\left(p_h^{n+1} - p_h^n\right)\right) = 0,\\
&\left(\mathbf{u}_h^{n+1}, \nabla\left(p_h^{n+1} - p_h^n\right)\right) = 0.
\end{aligned} \tag{46}$$

Summing up (46) gives

$$\left\|\tilde{\mathbf{u}}_h^{n+1}\right\|^2 = \left\|\mathbf{u}_h^{n+1}\right\|^2 + \tau^2\left\|\nabla\left(p_h^{n+1} - p_h^n\right)\right\|^2. \tag{47}$$

Finally, plugging (47) into (45) yields

$$\begin{aligned}
&\frac{1}{2}\left\|\mathbf{u}_h^{n+1}\right\|^2 + \frac{\lambda}{2}\left\|\nabla\phi_h^{n+1}\right\|^2 + \lambda\left\|U^{n+1}\right\|^2 + \frac{\tau^2}{2}\left\|\nabla p_h^{n+1}\right\|^2\\
&+\tau\gamma\left\|\nabla w_h^{n+1}\right\|^2 + \frac{\lambda}{2}\left\|\nabla\left(\phi_h^{n+1} - \phi_h^n\right)\right\|^2 + \lambda\left\|U^{n+1} - U_h^n\right\|^2\\
&+\frac{1}{2}\left\|\hat{\mathbf{u}}^{n+1} - \mathbf{u}_h^n\right\|^2 + \frac{1}{2}\left\|\tilde{\mathbf{u}}_h^{n+1} - \hat{\mathbf{u}}^{n+1}\right\|^2 + \tau\mu\left\|\nabla\tilde{\mathbf{u}}_h^{n+1}\right\|^2\\
&= \frac{1}{2}\|\mathbf{u}_h^n\|^2 + \frac{\lambda}{2}\|\nabla\phi_h^n\|^2 + \lambda\|U_h^n\|^2 + \frac{\tau^2}{2}\|\nabla p_h^n\|^2,
\end{aligned} \tag{48}$$

which establishes the energy stability (36). □

3.1.2. C-BDF1 scheme. An alternative first-order, fully discrete IEQ-FEM schemereferred to as the C-BDF1 schemeis formulated by retaining the intermediate function U^n from the P-BDF1 scheme (24)-(26) in continuous function space $C^0(\Omega)$. Specifically, the scheme seeks functions $U^{n+1} \in C^0(\Omega)$, $\hat{\mathbf{u}}^{\mathbf{n+1}} \in (L^2(\Omega))^d$, and $(\phi_h^{n+1}, w_h^{n+1}, \tilde{\mathbf{u}}_h^{n+1}, p_h^{n+1}) \in Y_h \times Y_h \times \mathbf{X}_h \times M_h$ such that

$$\left(\frac{\phi_h^{n+1} - \phi_h^n}{\tau}, \varphi_h\right) - \left(\left(\hat{\mathbf{u}}^{n+1}\phi_h^n\right), \nabla\varphi_h\right) + \gamma a\left(w_h^{n+1}, \varphi_h\right) = 0, \qquad \forall\varphi_h \in Y_h, \tag{49a}$$

$$\left(w_h^{n+1}, \psi_h\right) - \lambda a\left(\phi_h^{n+1}, \psi_h\right) - \lambda\left(H\left(\phi_h^n\right)U^{n+1}, \psi_h\right) = 0, \qquad \forall\psi_h \in Y_h, \tag{49b}$$

$$\hat{\mathbf{u}}^{n+1} = \mathbf{u}_h^n - \tau\phi_h^n\nabla w_h^{n+1}, \tag{49c}$$

$$U^{n+1} = U^n + \frac{1}{2}H\left(\phi_h^n\right)\left(\phi_h^{n+1} - \phi_h^n\right), \tag{49d}$$

(50)
$$\left(\frac{\tilde{\mathbf{u}}_h^{n+1}-\mathbf{u}_h^n}{\tau},\mathbf{v}_h\right)+\mu\tilde{a}\left(\tilde{\mathbf{u}}_h^{n+1},\mathbf{v}_h\right)+b\left(\mathbf{u}_h^n,\tilde{\mathbf{u}}_h^{n+1},\mathbf{v}_h\right)-\left(p_h^n,\nabla\cdot\mathbf{v}_h\right)$$
$$+\left(\phi_h^n\nabla w_h^{n+1},\mathbf{v}_h\right)=0,\qquad\forall\mathbf{v}_h\in\mathbf{X}_h,$$

and

$$\left(\frac{\mathbf{u}_h^{n+1}-\tilde{\mathbf{u}}_h^{n+1}}{\tau},\chi_h\right)-\left(\left(p_h^{n+1}-p_h^n\right),\nabla\cdot\chi_h\right)=0,\qquad\forall\chi_h\in\mathbf{V}_h,\tag{51}$$
$$\left(\nabla\cdot\mathbf{u}_h^{n+1},q_h\right)=0,\qquad\forall q_h\in M_h.$$

Similar to the P-BDF1 scheme (24)-(26), the initial data set $(\phi_h^0,\mathbf{u}_h^0,U^0)$ is given by (7) and (13). Additionally, we have the following result.

Remark 3.9. The main difference between the C-BDF1 scheme (49)–(51) and the P-BDF1 scheme (24)–(26) lies in equations (49d) and (24e). Specifically, the right-hand side of (49d) does not enforce the previous-step auxiliary variable U^n to lie in the finite element space.

Theorem 3.10. *For the CHNS equations* (1)*, the C-BDF1 scheme* (49)-(51) *is unconditionally energy stable and satisfies the following modified discrete energy law:*

$$\begin{aligned}&E\left(\phi_h^{n+1},\mathbf{u}_h^{n+1},U^{n+1},p_h^{n+1}\right)\\&=E\left(\phi_h^n,\mathbf{u}_h^n,U^n,p_h^n\right)-\tau\gamma\left\|\nabla w_h^{n+1}\right\|^2-\frac{\lambda}{2}\left\|\nabla\left(\phi_h^{n+1}-\phi_h^n\right)\right\|^2\\&-\lambda\left\|U^{n+1}-U^n\right\|^2-\frac{1}{2}\left\|\hat{\mathbf{u}}^{n+1}-\mathbf{u}_h^n\right\|^2\\&-\frac{1}{2}\left\|\tilde{\mathbf{u}}_h^{n+1}-\hat{\mathbf{u}}^{n+1}\right\|^2-\tau\mu\left\|\nabla\tilde{\mathbf{u}}_h^{n+1}\right\|^2,\end{aligned}\tag{52}$$

where

$$E\left(\phi_h^{n+1},\mathbf{u}_h^{n+1},U^{n+1},p_h^{n+1}\right)=\mathcal{E}\left(\phi_h^{n+1},\mathbf{u}_h^{n+1},U^{n+1}\right)+\frac{\tau^2}{2}\left\|\nabla p_h^{n+1}\right\|,$$

and $\mathcal{E}\left(\phi_h^{n+1},\mathbf{u}_h^{n+1},U^{n+1}\right)$ *is defined in equation* (11).

The proof of Theorem 3.10 is similar to that of Theorem 3.8.

The C-BDF1 scheme offers a computationally efficient alternative while still preserving the energy dissipation law (52). However, the exact computation of the discrete energy $E(\phi_h^n,\mathbf{u}_h^n,U^n,p_h^n)$ is no longer feasible, since $U^n\notin Y_h$. Instead, the energy must be approximated by $E(\phi_h^n,\mathbf{u}_h^n,U_I^n,p_h^n)$, where $U_I^n\in Y_h$ denotes the interpolation of U^n evaluated at Gaussian quadrature points.

Remark 3.11. At each time step, the following identity holds:

$$E\left(\phi_h^n,\mathbf{u}_h^n,U^n,p_h^n\right)=E\left(\phi_h^n,\mathbf{u}_h^n,U_I^n,p_h^n\right)+\lambda(\|U^n\|^2-\|U_I^n\|^2).\tag{53}$$

Based on this relation (53), the discrete energy dissipation law (52) can be equivalently expressed in terms of the approximated energy as:

(54)
$$\begin{aligned}&E\left(\phi_h^{n+1},\mathbf{u}_h^{n+1},U_I^{n+1},p_h^{n+1}\right)-E\left(\phi_h^n,\mathbf{u}_h^n,U_I^n,p_h^n\right)\\&=-\tau\gamma\left\|\nabla w_h^{n+1}\right\|^2-\frac{\lambda}{2}\left\|\nabla\left(\phi_h^{n+1}-\phi_h^n\right)\right\|^2-\lambda\left\|U^{n+1}-U^n\right\|^2-\frac{1}{2}\left\|\hat{\mathbf{u}}^{n+1}-\mathbf{u}_h^n\right\|^2\\&-\frac{1}{2}\left\|\tilde{\mathbf{u}}_h^{n+1}-\hat{\mathbf{u}}^{n+1}\right\|^2-\tau\mu\left\|\nabla\tilde{\mathbf{u}}_h^{n+1}\right\|^2+\lambda(\|U_I^{n+1}\|^2-\|U_I^n\|^2-\|U^{n+1}\|^2+\|U^n\|^2).\end{aligned}$$

However, the decay of the approximated energy may not be guaranteed if the last term in (54) becomes positive and dominant.

Remark 3.12. The error between the discrete energy $E(\phi_h^n, \mathbf{u}_h^n, U^n, p_h^n)$ in Theorem 3.10 and the approximated energy $E(\phi_h^n, \mathbf{u}_h^n, U_I^n, p_h^n)$ satisfies

$$|E(\phi_h^n, \mathbf{u}_h^n, U^n, p_h^n) - E(\phi_h^n, \mathbf{u}_h^n, U_I^n, p_h^n)| \leq \lambda(\|U^n\| + \|U_I^n\|)(\|U^n - U_I^n\|). \tag{55}$$

where the interpolation error $\|U^n - U_I^n\|$ may be reduced by refining meshes or adjusting the constant B to an appropriate larger number [19].

3.1.3. CP-BDF1 scheme. The C-BDF1 scheme is straightforward to implement and stands out as the most computationally efficient. However, as noted in Remark 3.12, its approximated energy in V_h is only conditionally dissipative. On the other hand, the P-BDF1 scheme includes an additional projection step compared to the C-BDF1 scheme, but it ensures unconditional energy dissipation, which can be directly computed in V_h.

To maintain the advantages of both methods, we design a hybrid CP-BDF1 scheme, which starts with the C-BDF1 scheme and switches to the P-BDF1 scheme at time $t_n = t_*$ if the approximated energy increases, i.e., $E(\phi_h^{n+1}, \mathbf{u}_h^{n+1}, U_I^{n+1}, p_h^{n+1}) > E(\phi_h^n, \mathbf{u}_h^n, U_I^n, p_h^n)$. The detailed algorithm is presented in Algorithm 1.

Algorithm 1 The CP-BDF1 scheme

Start with time step τ, total time T and initial solution $(\phi_h^0, \mathbf{u}_h^0, p_h^0, U^0)$;
Set $n = 0$ and $t_0 = 0$;
Compute the energy $E_h^0 = E\left(\phi_h^0, \mathbf{u}_h^0, U_I^0, p_h^0\right)$;
for $0 \leq n \leq \frac{T}{\tau}$ **do**
  Set $t_{n+1} = t_n + \tau$;
  Solve $(\phi_h^{n+1}, w_h^{n+1}, \mathbf{u}_h^{n+1}, p_h^{n+1})$ and U_I^{n+1} by using the C-BDF1 scheme;
  Compute the energy $E_h^{n+1} = E\left(\phi_h^{n+1}, \mathbf{u}_h^{n+1}, U_I^{n+1}, p_h^{n+1}\right)$;
  if $E_h^{n+1} > E_h^n$ **then**
    Store $n^* = n$, $(\phi_h^n, w_h^n, \mathbf{u}_h^n, p_h^n)$ and U_I^n;
    Break;
  end if
  $n = n + 1$;
end for
for $n^* \leq n \leq \frac{T}{\tau}$ **do**
  Set $t_{n+1} = t_n + \tau$;
  Compute the L^2 projection U_h^n of U_I^n in the finite element space Y_h;
  Solve $(\phi_h^{n+1}, w_h^{n+1}, \mathbf{u}_h^{n+1}, p_h^{n+1})$ and U_h^{n+1} by using the P-BDF1 scheme;
  Compute the energy $E_h^{n+1} = E\left(\phi_h^{n+1}, \mathbf{u}_h^{n+1}, U_h^{n+1}, p_h^{n+1}\right)$;
  $n = n + 1$;
end for

Theorem 3.13. *For $n \geq 0$, let E_h^n be the discrete energy of the solution from the hybrid CP-BDF1 scheme at t_n. Then it holds*

$$E_h^{n+1} \leq E_h^n, \tag{56}$$

where the approximated energy

$$E_h^n = E(\phi_h^n, \mathbf{u}_h^n, U_I^n, p_h^n)$$

for $n \le n^*$, and

$$E_h^n = E(\phi_h^n, \mathbf{u}_h^n, U_h^n, p_h^n)$$

for $n > n^*$, where n^* given in Algorithm 1.

Proof. Algorithm 1 together with Theorem 3.10 and Remark 3.12 implies that (56) holds for $n < n^*$, namely

$$E(\phi_h^{n+1}, \mathbf{u}_h^{n+1}, U_I^{n+1}, p_h^{n+1}) \le E(\phi_h^n, \mathbf{u}_h^n, U_I^n, p_h^n).$$

Theorem 3.8 implies that (56) also holds for $n > n^*$. To this end, we only need to prove that (56) holds for $n = n^*$. Recall that

$$E_h^{n^*} = E(\phi_h^{n^*}, \mathbf{u}_h^{n^*}, U_I^{n^*}, p_h^{n^*}), \tag{57}$$

$$E_h^{n^*+1} = E(\phi_h^{n^*+1}, \mathbf{u}_h^{n^*+1}, U_h^{n^*+1}, p_h^{n^*+1}). \tag{58}$$

Also recall that $U_h^{n^*+1}$ is obtained in the following steps

$$\left(U_h^{n^*}, \mu_h\right) = \left(U_I^{n^*}, \mu_h\right), \qquad \forall \mu_h \in Y_h, \tag{59}$$

$$U^{n^*+1} = U_h^{n^*} + \frac{1}{2} H\left(\phi_h^{n^*}\right)\left(\phi_h^{n^*+1} - \phi_h^{n^*}\right), \tag{60}$$

$$\left(U_h^{n^*+1}, \mu_h\right) = \left(U^{n^*+1}, \mu_h\right), \qquad \forall \mu_h \in Y_h. \tag{61}$$

Here, (59) gives

$$E(\phi_h^{n^*}, \mathbf{u}_h^{n^*}, U_h^{n^*}, p_h^{n^*}) \le E(\phi_h^{n^*}, \mathbf{u}_h^{n^*}, U_I^{n^*}, p_h^{n^*}). \tag{62}$$

Similar to Theorem 3.8, (60) and (61) together with scheme (24)-(26) yield

$$\begin{aligned} E\left(\phi_h^{n^*+1}, \mathbf{u}_h^{n^*+1}, U_h^{n^*+1}, p_h^{n^*+1}\right) &\le E\left(\phi_h^{n^*+1}, \mathbf{u}_h^{n^*+1}, U^{n^*+1}, p_h^{n^*+1}\right) \\ &\le E\left(\phi_h^{n^*}, \mathbf{u}_h^{n^*}, U_h^{n^*}, p_h^{n^*}\right). \end{aligned} \tag{63}$$

Finally, (62) and (63) imply that (56) holds $n = n^*$. □

Remark 3.14. The CP-BDF1 scheme in Algorithm 1 combines the computational efficiency of the C-BDF1 scheme with the unconditional energy stability of the P-BDF1 scheme.

3.2. Second order fully discrete schemes.

3.2.1. P-BDF2 scheme. In this subsection, we present the second order fully discrete IEQ-FEM scheme with intermediate function in polynomial space (P-BDF2 scheme) for the CHNS equations.

Motivated by the techniques for the P-BDF1 scheme, we consider the following second order fully discrete backward time-differentiation formula (BDF2) for the CHNS equations by approximating the intermediate function $U^{n+1} \in C^0(\Omega)$ and

functions $(\phi_h^{n+1}, w_h^{n+1}, \tilde{\mathbf{u}}_h^{n+1}, \mathbf{u}_h^{n+1}, p_h^{n+1}) \in Y_h \times Y_h \times \mathbf{X}_h \times \mathbf{V}_h \times M_h$, such that

$$\left(\frac{3\phi_h^{n+1} - 4\phi_h^n + \phi_h^{n-1}}{2\tau}, \varphi_h\right) - \left(\left(\tilde{\mathbf{u}}_h^{n+1}\phi_h^{n,\star}\right), \nabla\varphi_h\right)$$

$$+\gamma a\left(w_h^{n+1}, \varphi_h\right) = 0, \qquad \forall \varphi_h \in Y_h, \tag{64a}$$

$$\left(w_h^{n+1}, \psi_h\right) - \lambda a\left(\phi_h^{n+1}, \psi_h\right) - \lambda\left(H\left(\phi_h^{n,\star}\right)U^{n+1}, \psi_h\right) = 0, \qquad \forall \psi_h \in Y_h, \tag{64b}$$

$$\left(\frac{3\tilde{\mathbf{u}}_h^{n+1} - 4\mathbf{u}_h^n + \mathbf{u}_h^{n-1}}{2\tau}, \mathbf{v}_h\right) + \mu\tilde{a}\left(\tilde{\mathbf{u}}_h^{n+1}, \mathbf{v}_h\right) + b\left(\mathbf{u}_h^{n,\star}, \tilde{\mathbf{u}}_h^{n+1}, \mathbf{v}_h\right)$$

$$-\left(p_h^n, \nabla\cdot\mathbf{v}_h\right) + \left(\phi_h^{n,\star}\nabla w_h^{n+1}, \mathbf{v}_h\right) = 0, \qquad \forall \mathbf{v}_h \in \mathbf{X}_h, \tag{64c}$$

$$\left(U_h^n, \mu_h\right) = \left(U^n, \mu_h\right), \qquad \forall \mu_h \in Y_h, \tag{64d}$$

(64e)

$$U^{n+1} = \frac{4U_h^n - U_h^{n-1}}{3} + \frac{1}{2}H\left(\phi_h^{n,\star}\right)\left(\frac{3\phi_h^{n+1} - 4\phi_h^n + \phi_h^{n-1}}{3}\right),$$

and

$$\left(\frac{3\mathbf{u}_h^{n+1} - 3\tilde{\mathbf{u}}_h^{n+1}}{2\tau}, \chi_h\right) - \left(\left(p_h^{n+1} - p_h^n\right), \nabla\cdot\chi_h\right) = 0, \qquad \forall \chi_h \in \mathbf{V}_h, \tag{65}$$

$$\left(\nabla\cdot\mathbf{u}_h^{n+1}, q_h\right) = 0, \qquad \forall q_h \in M_h,$$

where $v_h^{n,\star}$ is defined as

$$v_h^{n,\star} = 2v_h^n - v_h^{n-1}.$$

The initial data set $(\phi_h^0, \mathbf{u}_h^0, U^0)$ is given by (7) and (13), and the first-step values $(\phi_h^1, \mathbf{u}_h^1, U^1)$ are obtained by using the P-BDF1 scheme (24)-(26).

Lemma 3.15. [18] *For any symmetric bilinear form $A(\cdot,\cdot)$, it satisfies*

$$\begin{aligned} A(\phi+\psi, \phi-\psi) =& A(\phi,\phi) - A(\psi,\psi), \\ 2A\left(3\phi_1 - 2\phi_2 - \phi_3, \phi_1\right) =& A\left(\phi_1,\phi_1\right) + A\left(2\phi_1 - \phi_2, 2\phi_1 - \phi_2\right) - A\left(\phi_2,\phi_2\right) \\ &+ A\left(\phi_1 - \phi_3, \phi_1 - \phi_3\right) - A\left(\phi_3,\phi_3\right), \end{aligned} \tag{66}$$

where $\phi,\ \psi,\ \phi_1,\ \phi_2,\ \phi_3 \in \mathbf{V}_h$.

Next, similar to the P-BDF1 scheme (24)-(26), the following result holds for the P-BDF2 scheme (64)-(65).

Theorem 3.16. *The P-BDF2 scheme* (64)-(65) *satisfies the following energy dissipation law*

$$\begin{aligned} &\bar{E}\left(\phi_h^{n+1}, \phi_h^{n+1,\star}, \mathbf{u}_h^{n+1}, \mathbf{u}_h^{n+1,\star}, U_h^{n+1}, U_h^{n+1,\star}, p_h^{n+1}\right) \\ &\le \bar{E}\left(\phi_h^{n+1}, \phi_h^{n+1,\star}, \mathbf{u}_h^{n+1}, \mathbf{u}_h^{n+1,\star}, 2U^{n+1} - U_h^n, p_h^{n+1}\right) \\ &= \bar{E}\left(\phi_h^n, \phi_h^{n,\star}, \mathbf{u}_h^n, \mathbf{u}_h^{n,\star}, U_h^n, U_h^{n,\star}, p_h^n\right) - 2\tau\mu\left\|\nabla\tilde{\mathbf{u}}_h^{n+1}\right\|^2 - 2\tau\gamma\left\|\nabla w_h^{n+1}\right\|^2 \\ &\quad - \frac{\lambda}{2}\left\|\nabla\left(\phi_h^{n+1} - \phi_h^{n,\star}\right)\right\|^2 - \lambda\left\|U^{n+1} - U_h^{n,\star}\right\|^2 - \frac{1}{2}\left\|\mathbf{u}_h^{n+1} - \mathbf{u}_h^{n,\star}\right\|^2 \\ &\quad - \frac{2\tau^2}{3}\left\|\nabla\left(p_h^{n+1} - p_h^n\right)\right\|^2, \end{aligned} \tag{67}$$

where

(68)
$$\bar{E}\left(\phi_h^n, \phi_h^{n,\star}, \mathbf{u}_h^n, \mathbf{u}_h^{n,\star}, U_h^n, U_h^{n,\star}, p_h^n\right) = \frac{\lambda}{2}\left(\|\nabla\phi_h^n\|^2 + \left\|\nabla\phi_h^{n,\star}\right\|^2\right) + \lambda\left(\|U_h^n\|^2 + \left\|U_h^{n,\star}\right\|^2\right) + \frac{1}{2}\left(\|\mathbf{u}_h^n\|^2 + \left\|\mathbf{u}_h^{n,\star}\right\|^2\right) + \frac{2\tau^2}{3}\|\nabla p_h^n\|^2.$$

Proof. Firstly, let $\varphi_h = 2\tau w_h^{n+1},\ \psi_h = -\left(3\phi_h^{n+1} - 4\phi_h^n + \phi_h^{n-1}\right),\ \mathbf{v}_h = 2\tau\tilde{\mathbf{u}}_h^{n+1}$ in (64a)-(64c), respectively. Then, it follows

(69)
$$\begin{aligned}
&\left(3\phi_h^{n+1} - 4\phi_h^n + \phi_h^{n-1}, w_h^{n+1}\right) + 2\tau\left(\nabla\cdot\left(\tilde{\mathbf{u}}_h^{n+1}\phi_h^{n,\star}\right), w_h^{n+1}\right)\\
&\quad + 2\tau\gamma a\left(w_h^{n+1}, w_h^{n+1}\right) = 0,\\
&-\left(w_h^{n+1}, 3\phi_h^{n+1} - 4\phi_h^n + \phi_h^{n-1}\right) + \lambda a\left(\phi_h^{n+1}, 3\phi_h^{n+1} - 4\phi_h^n + \phi_h^{n-1}\right)\\
&\quad + \lambda\left(H\left(\phi_h^{n,\star}\right)U^{n+1}, 3\phi_h^{n+1} - 4\phi_h^n + \phi_h^{n-1}\right) = 0,\\
&\left(3\tilde{\mathbf{u}}_h^{n+1} - 4\mathbf{u}_h^n + \mathbf{u}_h^{n-1}, \tilde{\mathbf{u}}_h^{n+1}\right) + 2\tau\mu\tilde{a}\left(\tilde{\mathbf{u}}_h^{n+1}, \tilde{\mathbf{u}}_h^{n+1}\right) - 2\tau\left(p_h^n, \nabla\cdot\tilde{\mathbf{u}}_h^{n+1}\right)\\
&\quad + 2\tau\left(\phi_h^{n,\star}\nabla w_h^{n+1}, \tilde{\mathbf{u}}_h^{n+1}\right) = 0.
\end{aligned}$$

The summation of (69) with using (64e) upon regrouping gives

(70)
$$\begin{aligned}
&2\tau\gamma\left\|\nabla w_h^{n+1}\right\|^2 + \lambda a\left(\phi_h^{n+1}, 3\phi_h^{n+1} - 4\phi_h^n + \phi_h^{n-1}\right)\\
&\quad + 2\lambda\left(U^{n+1}, 3U^{n+1} - 4U_h^n + U_h^{n-1}\right)\\
&+\left(3\mathbf{u}_h^{n+1} - 4\mathbf{u}_h^n + \mathbf{u}_h^{n-1}, \tilde{\mathbf{u}}_h^{n+1}\right) + \left(3\tilde{\mathbf{u}}_h^{n+1} - 3\mathbf{u}_h^{n+1}, \tilde{\mathbf{u}}_h^{n+1} + \mathbf{u}_h^{n+1}\right)\\
&\quad + 2\tau\mu\left\|\nabla\tilde{\mathbf{u}}_h^{n+1}\right\| - 2\tau\left(p_h^n, \nabla\cdot\tilde{\mathbf{u}}_h^{n+1}\right) = 0,
\end{aligned}$$

where we have used the identity $\left(3\tilde{\mathbf{u}}_h^{n+1} - 3\mathbf{u}_h^{n+1}, \mathbf{u}_h^{n+1}\right) = 0$, which follows by choosing $\chi_h = 2\tau\mathbf{u}_h^{n+1}$ and $q_h = 2\tau\nabla(p_h^{n+1} - p_h^n)$ in equation (65). Then according to Lemma 3.15, and

(71)
$$\left(3\mathbf{u}_h^{n+1} - 4\mathbf{u}_h^n + \mathbf{u}_h^{n-1}, \tilde{\mathbf{u}}_h^{n+1}\right) = \left(3\mathbf{u}_h^{n+1} - 4\mathbf{u}_h^n + \mathbf{u}_h^{n-1}, \mathbf{u}_h^{n+1}\right),$$

which follows by choosing $\chi_h = 2\tau(3\mathbf{u}_h^{n+1} - 4\mathbf{u}_h^n + \mathbf{u}_h^{n-1})$ in equation (65), it holds

(72)
$$\begin{aligned}
&2\tau\gamma\left\|\nabla w_h^{n+1}\right\|^2 + 2\tau\mu\left\|\nabla\tilde{\mathbf{u}}_h^{n+1}\right\|^2 - 2\tau\left(p_h^n, \nabla\cdot\tilde{\mathbf{u}}_h^{n+1}\right)\\
&+\frac{\lambda}{2}\left(\left\|\nabla\phi_h^{n+1}\right\|^2 + \left\|\nabla\phi_h^{n+1,\star}\right\|^2 - \|\nabla\phi_h^n\|^2 - \left\|\nabla\phi_h^{n,\star}\right\|^2 + \left\|\nabla\left(\phi_h^{n+1} - \phi_h^{n,\star}\right)\right\|^2\right)\\
&+\lambda\left(\left\|U^{n+1}\right\|^2 + \left\|2U^{n+1} - U_h^n\right\|^2 - \|U_h^n\|^2 - \left\|U_h^{n,\star}\right\|^2 + \left\|U^{n+1} - U_h^{n,\star}\right\|^2\right)\\
&+\frac{1}{2}\left(\left\|\mathbf{u}_h^{n+1}\right\|^2 + \left\|\mathbf{u}_h^{n+1,\star}\right\|^2 - \|\mathbf{u}_h^n\|^2 - \left\|\mathbf{u}_h^{n,\star}\right\|^2 + \left\|\mathbf{u}_h^{n+1} - \mathbf{u}_h^{n,\star}\right\|^2\right)\\
&+3\left(\left\|\tilde{\mathbf{u}}_h^{n+1}\right\|^2 - \left\|\mathbf{u}_h^{n+1}\right\|^2\right) = 0,
\end{aligned}$$

here the properties of the numerical solution $\nabla\cdot\mathbf{u}^m = 0,\ m = 1, 2, \ldots, n+1$ is applied. Secondly, taking $\chi_h,\ q_h$ as $2\tau\nabla p_h^n,\ p_h^n$ in (65), respectively, we get

(73)
$$\begin{aligned}
\left(3\mathbf{u}_h^{n+1} - 3\tilde{\mathbf{u}}_h^{n+1}, \nabla p_h^n\right) + 2\tau\left(\nabla\left(p_h^{n+1} - p_h^n\right), \nabla p_h^n\right) = 0,\\
\left(\mathbf{u}_h^{n+1}, \nabla p_h^n\right) = 0,
\end{aligned}$$

which can be simplified as

(74)
$$-\left(3\tilde{\mathbf{u}}_h^{n+1}, \nabla p_h^n\right) + \tau\left(\left\|\nabla p_h^{n+1}\right\|^2 - \left\|\nabla\left(p_h^{n+1} - p_h^n\right)\right\|^2 - \|\nabla p_h^n\|^2\right) = 0.$$

Plugging (74) into (72) to replace $-2\tau\left(p_h^n, \nabla\cdot\tilde{\mathbf{u}}_h^{n+1}\right)$ yields

(75)
$$\begin{aligned}
&\frac{\lambda}{2}\left(\left\|\nabla\phi_h^{n+1}\right\|^2+\left\|\nabla\phi_h^{n+1,\star}\right\|^2-\left\|\nabla\phi_h^n\right\|^2-\left\|\nabla\phi_h^{n,\star}\right\|^2+\left\|\nabla\left(\phi_h^{n+1}-\phi_h^{n,\star}\right)\right\|^2\right)\\
&+\lambda\left(\left\|U^{n+1}\right\|^2+\left\|2U^{n+1}-U_h^n\right\|^2-\left\|U_h^n\right\|^2-\left\|U_h^{n,\star}\right\|^2+\left\|U^{n+1}-U_h^{n,\star}\right\|^2\right)\\
&+\frac{1}{2}\left(\left\|\mathbf{u}_h^{n+1}\right\|^2+\left\|\mathbf{u}_h^{n+1,\star}\right\|^2-\left\|\mathbf{u}_h^n\right\|^2-\left\|\mathbf{u}_h^{n,\star}\right\|^2+\left\|\mathbf{u}_h^{n+1}-\mathbf{u}_h^{n,\star}\right\|^2\right)\\
&+3\left(\left\|\tilde{\mathbf{u}}_h^{n+1}\right\|^2-\left\|\mathbf{u}_h^{n+1}\right\|^2\right)+2\tau\mu\left\|\nabla\tilde{\mathbf{u}}_h^{n+1}\right\|^2+2\tau\gamma\left\|\nabla w_h^{n+1}\right\|^2\\
&+\frac{2\tau^2}{3}\left(\left\|\nabla p_h^{n+1}\right\|^2-\left\|\nabla\left(p_h^{n+1}-p_h^n\right)\right\|^2-\left\|\nabla p_h^n\right\|^2\right)=0.
\end{aligned}$$

Finally, let $\chi_h=2\tau\left(\mathbf{u}_h^{n+1}+\tilde{\mathbf{u}}_h^{n+1}\right)$, $q_h=p_h^{n+1}-p_h^n$ in (65). Then,

$$\begin{aligned}
\left(3\mathbf{u}_h^{n+1}-3\tilde{\mathbf{u}}_h^{n+1},\mathbf{u}_h^{n+1}+\tilde{\mathbf{u}}_h^{n+1}\right)+2\tau\left(\nabla\left(p_h^{n+1}-p_h^n\right),\mathbf{u}_h^{n+1}+\tilde{\mathbf{u}}_h^{n+1}\right)=0,\\
\left(\mathbf{u}_h^{n+1},\nabla\left(p_h^{n+1}-p_h^n\right)\right)=0,
\end{aligned}\tag{76}$$

leading to

$$3\left\|\mathbf{u}_h^{n+1}\right\|^2-3\left\|\tilde{\mathbf{u}}_h^{n+1}\right\|^2+2\tau\left(\nabla\left(p_h^{n+1}-p_h^n\right),\tilde{\mathbf{u}}_h^{n+1}\right)=0.\tag{77}$$

In addition, taking $\chi_h=\tau\nabla\left(p_h^{n+1}-p_h^n\right)$ in (65) gives

$$\left(3\mathbf{u}_h^{n+1}-3\tilde{\mathbf{u}}_h^{n+1},\nabla\left(p_h^{n+1}-p_h^n\right)\right)+2\tau\left(\nabla\left(p_h^{n+1}-p_h^n\right),\nabla\left(p_h^{n+1}-p_h^n\right)\right)=0.\tag{78}$$

Upon simplification, it follows

$$\left(\tilde{\mathbf{u}}_h^{n+1},\nabla\left(p_h^{n+1}-p_h^n\right)\right)=\frac{2}{3}\tau\left(\nabla\left(p_h^{n+1}-p_h^n\right),\nabla\left(p_h^{n+1}-p_h^n\right)\right).\tag{79}$$

Plugging (79) into (77) gives

$$\left\|\tilde{\mathbf{u}}_h^{n+1}\right\|^2-\left\|\mathbf{u}_h^{n+1}\right\|^2=\frac{4}{9}\tau^2\left(\nabla\left(p_h^{n+1}-p_h^n\right),\nabla\left(p_h^{n+1}-p_h^n\right)\right).\tag{80}$$

By summing (80) with (75),

$$\begin{aligned}
&\frac{\lambda}{2}\left(\left\|\nabla\phi_h^{n+1}\right\|^2+\left\|\nabla\phi_h^{n+1,\star}\right\|^2\right)+\lambda\left(\left\|U^{n+1}\right\|^2+\left\|2U^{n+1}-U_h^n\right\|^2\right)\\
&+\frac{1}{2}\left(\left\|\mathbf{u}_h^{n+1}\right\|^2+\left\|\mathbf{u}_h^{n+1,\star}\right\|^2\right)+\frac{2\tau^2}{3}\left\|\nabla p_h^{n+1}\right\|^2\\
&+2\tau\mu\left\|\nabla\tilde{\mathbf{u}}_h^{n+1}\right\|^2+2\tau\gamma\left\|\nabla w_h^{n+1}\right\|^2+\frac{\lambda}{2}\left\|\nabla\left(\phi_h^{n+1}-\phi_h^{n,\star}\right)\right\|^2\\
&+\lambda\left\|U^{n+1}-U_h^{n,\star}\right\|^2+\frac{1}{2}\left\|\mathbf{u}_h^{n+1}-\mathbf{u}_h^{n,\star}\right\|^2+\frac{2\tau^2}{3}\left\|\nabla\left(p_h^{n+1}-p_h^n\right)\right\|^2\\
&=\frac{\lambda}{2}\left(\left\|\nabla\phi_h^n\right\|^2+\left\|\nabla\phi_h^{n,\star}\right\|^2\right)+\lambda\left(\left\|U_h^n\right\|^2+\left\|U_h^{n,\star}\right\|^2\right)\\
&+\frac{1}{2}\left(\left\|\mathbf{u}_h^n\right\|^2+\left\|\mathbf{u}_h^{n,\star}\right\|^2\right)+\frac{2\tau^2}{3}\left\|\nabla p_h^n\right\|^2.
\end{aligned}\tag{81}$$

Based on the stability property of the L^2 projection,

$$\|U_h^{n+1}\|\le\|U^{n+1}\|,$$

and the following fact

$$\left(2U_h^{n+1}-U_h^n,\mu_h\right)=\left(2U^{n+1}-U_h^n,\mu_h\right),\qquad\forall\mu_h\in Y_h$$

implies the desired result (67). □

3.2.2. C-BDF2 scheme. We also process with another second-order fully discrete IEQ-FEM scheme (C-BDF2 scheme) for CHNS equations by approximating the intermediate function $U^{n+1} \in C^0(\Omega)$ and functions $(\phi_h^{n+1}, w_h^{n+1}, \tilde{\mathbf{u}}_h^{n+1}, \mathbf{u}_h^{n+1}, p_h^{n+1}) \in Y_h \times Y_h \times \mathbf{X}_h \times \mathbf{V}_h \times M_h$, such that

$$\left(\frac{3\phi_h^{n+1} - 4\phi_h^n + \phi_h^{n-1}}{2\tau}, \varphi_h\right) - \left(\left(\tilde{\mathbf{u}}_h^{n+1}\phi_h^{n,\star}\right), \nabla\varphi_h\right)$$

$$+\gamma a\left(w_h^{n+1}, \varphi_h\right) = 0, \qquad \forall \varphi_h \in Y_h, \tag{82a}$$

$$\left(w_h^{n+1}, \psi_h\right) - \lambda a\left(\phi_h^{n+1}, \psi_h\right) - \lambda\left(H\left(\phi_h^{n,\star}\right)U^{n+1}, \psi_h\right) = 0, \qquad \forall \psi_h \in Y_h, \tag{82b}$$

$$\left(\frac{3\tilde{\mathbf{u}}_h^{n+1} - 4\mathbf{u}_h^n + \mathbf{u}_h^{n-1}}{2\tau}, \mathbf{v}_h\right) + \mu\tilde{a}\left(\tilde{\mathbf{u}}_h^{n+1}, \mathbf{v}_h\right) + b\left(\mathbf{u}_h^{n,\star}, \tilde{\mathbf{u}}_h^{n+1}, \mathbf{v}_h\right)$$

$$-\left(p_h^n, \nabla\cdot\mathbf{v}_h\right) + \left(\phi_h^{n,\star}\nabla w_h^{n+1}, \mathbf{v}_h\right) = 0, \qquad \forall \mathbf{v}_h \in \mathbf{X}_h, \tag{82c}$$

$$U^{n+1} = \frac{4U^n - U^{n-1}}{3} + \frac{1}{2}H\left(\phi_h^{n,\star}\right)\left(\frac{3\phi_h^{n+1} - 4\phi_h^n + \phi_h^{n-1}}{3}\right), \tag{82d}$$

and

$$\left(\frac{3\mathbf{u}_h^{n+1} - 3\tilde{\mathbf{u}}_h^{n+1}}{2\tau}, \chi_h\right) - \left(\left(p_h^{n+1} - p_h^n\right), \nabla\cdot\chi_h\right) = 0, \qquad \forall \chi_h \in \mathbf{V}_h,$$

$$\left(\nabla\cdot\mathbf{u}_h^{n+1}, q_h\right) = 0, \qquad \forall q_h \in M_h. \tag{83}$$

Similar to the P-BDF2 scheme, the initial data set $(\phi_h^0, \mathbf{u}_h^0, U^0)$ is given by (7) and (13), and the first-step values $(\phi_h^1, \mathbf{u}_h^1, U^1)$ are obtained using the C-BDF1 scheme (49)-(51).

Remark 3.17. The C-BDF2 scheme (82)-(83) first solves for $(\phi_h^{n+1}, w_h^{n+1}, \tilde{\mathbf{u}}_h^{n+1})$ by computing the coupled system. Compared with the C-BDF1 scheme (49)-(51), the C-BDF2 requires solving three unknown variables simultaneously, whereas the C-BDF1 involves at most two, which increases the CPU time.

The following result holds for the C-BDF2 scheme (82)-(83).

Lemma 3.18. *The C-BDF2 scheme* (82)-(83) *satisfies the following energy dissipation law*

$$\begin{aligned}
&\bar{E}\left(\phi_h^{n+1}, \phi_h^{n+1,\star}, \mathbf{u}_h^{n+1}, \mathbf{u}_h^{n+1,\star}, U^{n+1}, U^{n+1,\star}, p_h^{n+1}\right)\\
=&\bar{E}\left(\phi_h^n, \phi_h^{n,\star}, \mathbf{u}_h^n, \mathbf{u}_h^{n,\star}, U^n, U^{n,\star}, p_h^n\right) - 2\tau\mu\left\|\nabla\tilde{\mathbf{u}}_h^{n+1}\right\|^2 - 2\tau\gamma\left\|\nabla w_h^{n+1}\right\|^2\\
&-\frac{\lambda}{2}\left\|\nabla\left(\phi_h^{n+1} - \phi_h^{n,\star}\right)\right\|^2 - \lambda\left\|U^{n+1} - U^{n,\star}\right\|^2 - \frac{1}{2}\left\|\mathbf{u}_h^{n+1} - \mathbf{u}_h^{n,\star}\right\|^2\\
&-\frac{2\tau^2}{3}\left\|\nabla\left(p_h^{n+1} - p_h^n\right)\right\|^2,
\end{aligned} \tag{84}$$

where

$$\bar{E}\left(\phi_h^n, \phi_h^{n,\star}, \mathbf{u}_h^n, \mathbf{u}_h^{n,\star}, U^n, U^{n,\star}, p_h^n\right) = \frac{\lambda}{2}\left(\|\nabla\phi_h^n\|^2 + \left\|\nabla\phi_h^{n,\star}\right\|^2\right)$$

$$+\lambda\left(\|U^n\|^2 + \|U^{n,\star}\|^2\right) + \frac{1}{2}\left(\|\mathbf{u}_h^n\|^2 + \left\|\mathbf{u}_h^{n,\star}\right\|^2\right) + \frac{2\tau^2}{3}\|\nabla p_h^n\|^2, \tag{85}$$

with the term $v^{n+1,\star}$ *being defined as*

$$v^{n+1,\star} = 2v^{n+1} - v^n.$$

Remark 3.19. Similar to the CP-BDF1 scheme proposed in Algorithm 1, we can also present the CP-BDF2 scheme by combining the C-BDF2 scheme and the P-BDF2 scheme.

Remark 3.20. The numerical solution from the second-order CrankNicolson (CN) IEQ-FEM shows instability, a phenomenon that has also been observed in the CN-IEQ-DG method [18, 39] and the CN-IEQ-FEM [8] when solving the CH equation with logarithmic potential. Additionally, extending the current work to higher-order time discretizations [16] is a potential direction for future research. The investigation into these time discretizations, including adaptive time discretizations [36], in combination with the IEQ-FEMs, will be addressed in our future work.

4. Numerical examples

In this section, we present 2D and 3D numerical examples to validate the theoretical results presented in this paper. In implementation, we consider uniform triangular meshes in 2D, and quasi-uniform tetrahedral meshes in 3D for the following numerical examples. The 2D triangular meshes are mainly generated as follows: the domain $\Omega = I_x \times I_y$ is first divided into an $N_x \times N_y$ rectangles, each of which is subdivided into two equal triangles. The mesh size of the triangulation is identified by either the partition number $N = N_x = N_y$ in each direction or the mesh size $h = h_x = h_y$, where $h_x = |I_x|/N_x$ and $h_y = |I_y|/N_y$. 3D tetrahedral meshes are generated and identified similarly.

4.1. Convergent rates. In this part, we give an example to validate the temporal and spatial convergence rates of the proposed numerical schemes for the CHNS equations.

Example 4.1. In the first example, we consider the following CHNS equations

$$
\begin{aligned}
\partial_t \phi + \nabla \cdot (\mathbf{u}\phi) - \gamma \Delta w &= g(t,x,y), && \text{in } \Omega \times (0,T],\\
w + \lambda\left(\Delta \phi - f(\phi)\right) &= 0, && \text{in } \Omega \times (0,T],\\
\partial_t \mathbf{u} - \mu \Delta \mathbf{u} + (\mathbf{u}\cdot\nabla)\,\mathbf{u} + \nabla p + \phi \nabla w &= \mathbf{h}(t,x,y), && \text{in } \Omega \times (0,T],\\
\nabla \cdot \mathbf{u} &= 0, && \text{in } \Omega \times (0,T],\\
\mathbf{u}(\cdot,0) = \mathbf{u}_0,\ \phi(\cdot,0) &= \phi_0, && \text{in } \Omega \times \{t=0\},\\
\mathbf{u} = 0,\ \frac{\partial \phi}{\partial \nu} = 0,\ \frac{\partial w}{\partial \nu} &= 0, && \text{on } \partial\Omega \times (0,T],
\end{aligned}
\tag{86}
$$

with $\Omega = [0, 4\pi]^2$, the exact solution satisfies

$$
\begin{aligned}
\phi(t,x,y) &= \sin(t)\cos\left(\frac{x}{2}\right)\cos\left(\frac{y}{2}\right),\\
\mathbf{u}(t,x,y) &= \left(e^{-\frac{49t}{64}}\sin^2\left(\frac{x}{4}\right)\sin\left(\frac{y}{2}\right), -e^{-\frac{49t}{64}}\sin\left(\frac{x}{2}\right)\sin^2\left(\frac{y}{4}\right)\right)^{\top},\\
p(t,x,y) &= \cos\left(\frac{x}{2}\right)\sin\left(\frac{y}{2}\right)(1-\sin(t)),
\end{aligned}
\tag{87}
$$

the parameters $\epsilon = 1,\ \lambda = 1,\ \mu = 1,\ \gamma = 1,\ B = 50$, and the corresponding right terms $g(x,t),\ \mathbf{h}(x,t)$ can be obtained by taking the the exact solution (87) into (86).

The errors and convergent rates for spatial discretization and temporal discretization between the numerical solution and exact solution based on the P-BDF1 scheme

TABLE 1. **Example 4.1**, L^2, H^1 error and convergent rate of spatial discretization for the P-BDF1 scheme (24)-(26) with $\tau = 10^{-7}$, $T = 10^{-5}$.

	$\|\phi-\phi_h\|_{L^2}$		$\|\mathbf{u}-\mathbf{u}_h\|_{L^2}$		$\|\phi-\phi_h\|_{H^1}$		$\|\mathbf{u}-\mathbf{u}_h\|_{H^1}$	
$N=4$	1.733e-05	−−	2.742e-01	−−	9.544e-05	−−	7.499e-01	−−
$N=8$	3.442e-06	2.33	3.672e-02	2.90	2.643e-05	1.85	1.999e-01	1.91
$N=16$	5.338e-07	2.69	4.671e-03	2.97	6.710e-06	1.98	5.078e-02	1.98
$N=32$	7.275e-08	2.88	5.864e-04	2.99	1.678e-06	2.00	1.275e-02	1.99
$N=64$	9.286e-09	2.97	7.340e-05	3.00	4.211e-07	1.99	3.191e-03	2.00

TABLE 2. **Example 4.1**, L^2, H^1 error and convergent rate of temporal discretization for the P-BDF1 scheme (24)-(26) with $N = 160$, $T = 2$.

	$\|\phi-\phi_h\|_{L^2}$		$\|\mathbf{u}-\mathbf{u}_h\|_{L^2}$		$\|\phi-\phi_h\|_{H^1}$		$\|\mathbf{u}-\mathbf{u}_h\|_{H^1}$	
$\tau=0.04$	1.783e-01	−−	5.235e-02	−−	1.478e-01	−−	3.089e-02	−−
$\tau=0.02$	8.978e-02	0.99	2.633e-02	0.99	7.504e-02	0.98	1.530e-02	1.01
$\tau=0.01$	4.504e-02	1.00	1.320e-02	1.00	3.781e-02	0.99	7.646e-03	1.00
$\tau=0.005$	2.256e-02	1.00	6.610e-03	1.00	1.899e-02	0.99	3.839e-03	0.99

TABLE 3. **Example 4.1**, L^2, H^1 error and convergent rate of spatial discretization for the P-BDF2 scheme (64)-(65) with $\tau = 10^{-7}$, $T = 10^{-5}$.

	$\|\phi-\phi_h\|_{L^2}$		$\|\mathbf{u}-\mathbf{u}_h\|_{L^2}$		$\|\phi-\phi_h\|_{H^1}$		$\|\mathbf{u}-\mathbf{u}_h\|_{H^1}$	
$N=4$	1.733e-06	−−	2.743e-01	−−	9.545e-06	−−	7.499e-01	−−
$N=8$	3.442e-07	2.33	3.673e-02	2.90	2.648e-06	1.85	1.999e-01	1.91
$N=16$	5.313e-08	2.70	4.672e-03	2.97	6.782e-07	1.97	5.079e-02	1.98
$N=32$	7.196e-09	2.88	5.866e-04	2.99	1.684e-07	2.01	1.275e-02	1.99
$N=64$	9.267e-10	2.96	7.341e-05	3.00	4.211e-08	2.00	3.191e-03	2.00

TABLE 4. **Example 4.1**, L^2, H^1 error and convergent rate of temporal discretization for the P-BDF2 scheme (64)-(65) with $N = 160$, $T = 2$.

	$\|\phi-\phi_h\|_{L^2}$		$\|\mathbf{u}-\mathbf{u}_h\|_{L^2}$		$\|\phi-\phi_h\|_{H^1}$		$\|\mathbf{u}-\mathbf{u}_h\|_{H^1}$	
$\tau=0.4$	7.754e-01	−−	1.585e-01	−−	5.547e-01	−−	1.204e-01	−−
$\tau=0.2$	2.022e-01	1.94	3.969e-02	2.00	1.455e-01	1.93	3.467e-02	1.80
$\tau=0.1$	5.051e-02	2.00	1.008e-02	1.98	3.648e-02	2.00	1.103e-02	1.65
$\tau=0.05$	1.253e-02	2.01	2.551e-03	1.98	9.075e-03	2.01	3.341e-03	1.72

(24)-(26) and P-BDF2 scheme (64)-(65) are shown in Tables 1-4, respectively. From the Tables, we numerically verify that for the P-BDF1 scheme

(88)

$$\left\|\phi(t_{n+1})-\phi_h^{n+1}\right\|_{L^2(\Omega)} \approx O(h^3+\tau), \qquad \left\|\mathbf{u}(t_{n+1})-\mathbf{u}_h^{n+1}\right\|_{(L^2(\Omega))^2} \approx O(h^3+\tau),$$

$$\left|\phi(t_{n+1})-\phi_h^{n+1}\right|_{H^1(\Omega)} \approx O(h^2+\tau), \qquad \left|\mathbf{u}(t_{n+1})-\mathbf{u}_h^{n+1}\right|_{(H^1(\Omega))^2} \approx O(h^2+\tau),$$

TABLE 5. CPU time for 100 steps calculated using four schemes: (1) scheme (24)-(26); (2) scheme (64)-(65); (3) scheme (49)-(51); (4) scheme (82)-(83).

Example 4.2	P scheme	C scheme
BDF1	535.0966s	496.5006s
BDF2	2011.748s	1972.774s

and for the P-BDF2 scheme

(89)
$$\left\|\phi(t_{n+1})-\phi_h^{n+1}\right\|_{L^2(\Omega)}\approx O(h^3+\tau^2),\qquad \left\|\mathbf{u}(t_{n+1})-\mathbf{u}_h^{n+1}\right\|_{(L^2(\Omega))^2}\approx O(h^3+\tau^2),$$
$$\left|\phi(t_{n+1})-\phi_h^{n+1}\right|_{H^1(\Omega)}\approx O(h^2+\tau^2),\qquad \left|\mathbf{u}(t_{n+1})-\mathbf{u}_h^{n+1}\right|_{(H^1(\Omega))^2}\approx O(h^2+\tau^2),$$

which are consistent with the expectations.

4.2. Numerical solutions for the CHNS equations. In the following four examples, we numerically investigate the performance of the proposed IEQ-FEM schemes for solving the CHNS equations. We conduct the computation by using schemes (24)-(26) and (64)-(65) separately and present the results as phase fields and velocity fields. Besides, the energy dissipation and mass conservation phenomena are also displayed.

Example 4.2. [40] In this example, we consider the CHNS equations (1) with the domain $\Omega=[0,1]^2$ and the initial condition

$$\begin{aligned}\phi_0 =&1-\tanh\left(\frac{-r+\sqrt{(x-x_a)^2+(y-y_a)^2}}{2\epsilon}\right)\\ &-\tanh\left(\frac{-r+\sqrt{(x-x_b)^2+(y-y_b)^2}}{2\epsilon}\right),\\ \mathbf{u}_0=&[0,\ 0]^\top,\end{aligned}\tag{90}$$

where $x_a=0.5-\frac{r}{\sqrt{2}},\ y_a=0.5+\frac{r}{\sqrt{2}},\ x_b=0.5+\frac{r}{\sqrt{2}},\ y_b=0.5-\frac{r}{\sqrt{2}},\ r=0.15$. The parameters are chosen as $\gamma=\mu=\epsilon=0.01,\ \lambda=0.01\epsilon,\ B=100$. We set the partition number $N\times N=128\times 128$, and time step $\tau=5\times10^{-4}$ with total time $T=3.2$.

Figures 1-2 show the numerical solution of phase fields ϕ_h^{n+1} and velocity fields $\mathbf{u}_h^{n+1}$ by using the P-BDF1 scheme (24)-(26) and P-BDF2 scheme (64)-(65). From the pictures, we can see that the numerical solutions of phase fields and velocity fields obtained by the two schemes are almost identical. We can see that the patterns are comparable to those in [40]. The evolution of the discrete energy and total mass are shown in Figure 3. The results indicate that both two schemes preserve the total mass and satisfy the energy dissipation law.

Besides, we also compare the CPU time of four classes of schemes: (1) P-BDF1 scheme; (2) P-BDF2 scheme; (3) C-BDF1 scheme; (4) C-BDF2 scheme, and the corresponding results are shown in Table 5. The results show that the additional projection step (24d) for BDF1 scheme and (64d) for BDF2 scheme in the CHNS equations slightly increases the computation time, which is acceptable.

In the following, we further present more examples based on the P-BDF2 scheme to investigate the performance of the proposed methods.

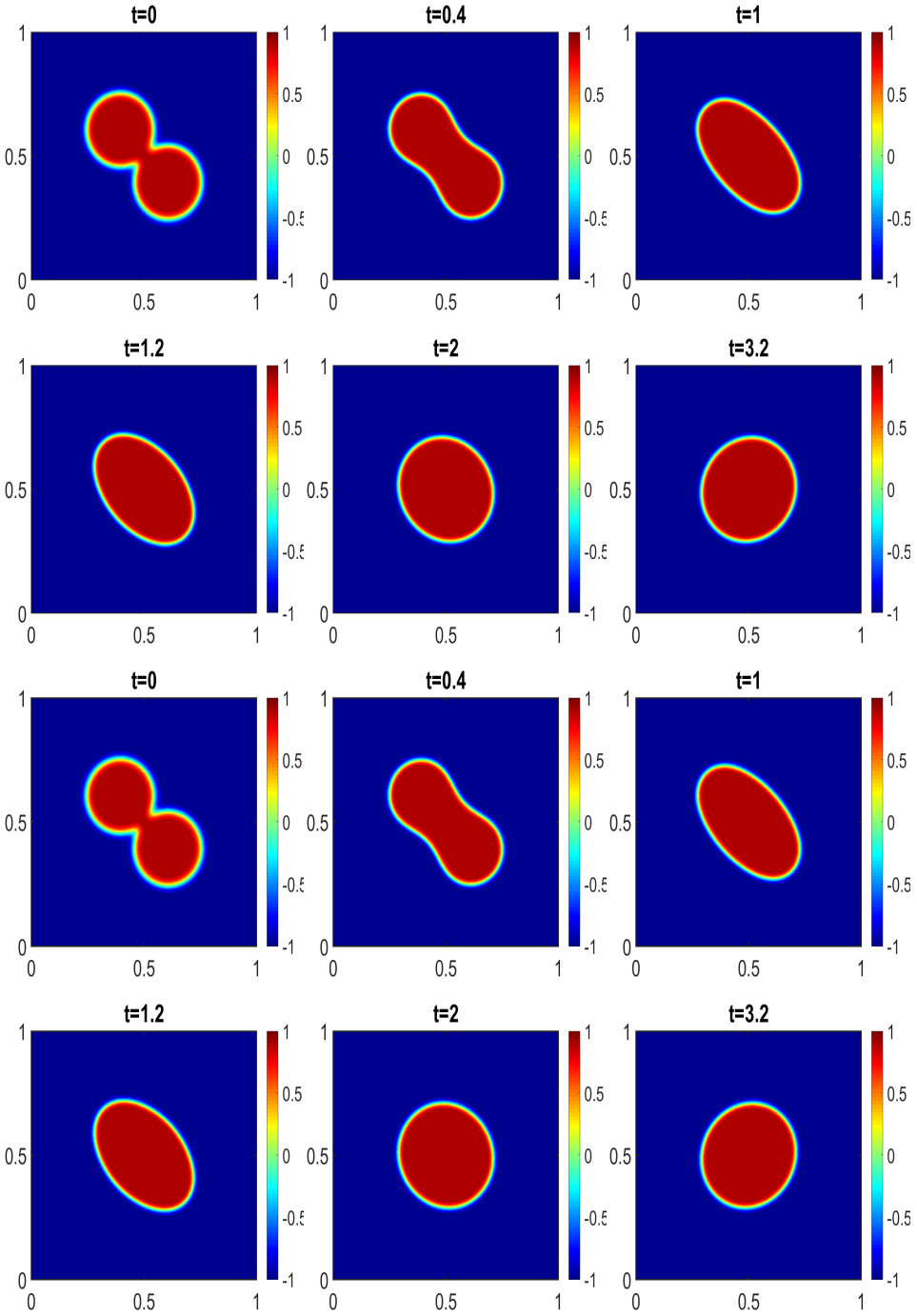

FIGURE 1. **Example 4.2**, snapshots of numerical solutions for phase fields function, First and second lines: P-BDF1 scheme (24)-(26); Third and fourth lines: P-BDF2 scheme (64)-(65).

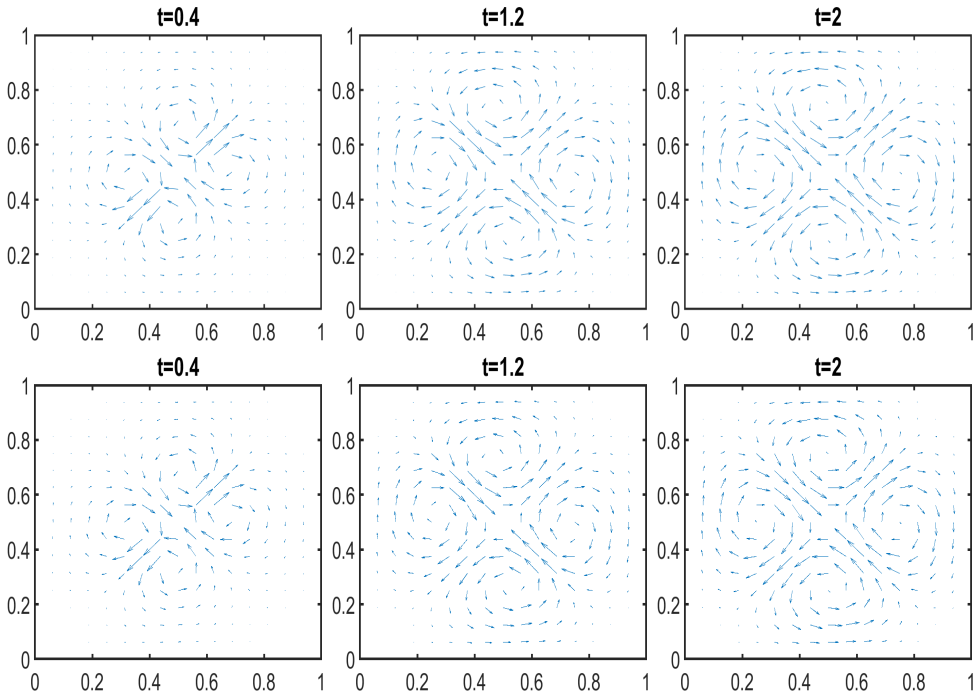

FIGURE 2. **Example 4.2**, snapshots of numerical solutions for velocity fields function, First line: P-BDF1 scheme (24)-(26); Second line: P-BDF2 scheme (64)-(65).

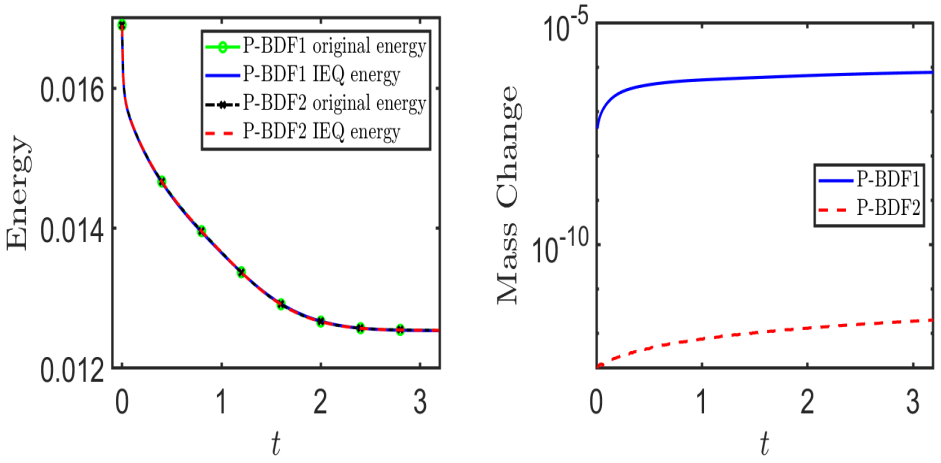

FIGURE 3. **Example 4.2**, the modified discrete energy history and discrete mass variation.

Example 4.3. In this example, we consider the CHNS equations (1) with the domain $\Omega = [-1,1]^2$ and the initial condition

(91)

$$\phi_0 = \tanh\left(\left((x-0.3)^2+y^2-0.2^2\right)/\epsilon^2\right) \times \tanh\left(\left((x+0.3)^2+y^2-0.2^2\right)/\epsilon^2\right) \times \tanh\left(\left(x^2+(y-0.3)^2-0.2^2\right)/\epsilon^2\right) \times \tanh\left(\left(x^2+(y+0.3)^2-0.2^2\right)/\epsilon^2\right),$$

$$\mathbf{u}_0 = \left[\sin(\pi x)^2 \sin(2\pi y), \quad \sin(2\pi x)\sin(\pi y)^2\right]^\top,$$

where the parameters $\epsilon = \lambda = 0.04$, $\mu = \gamma = 1$, $B = 50$, the mesh $N \times N = 80 \times 80$, time step $\tau = 10^{-6}$ and the final time $T = 10^{-1}$.

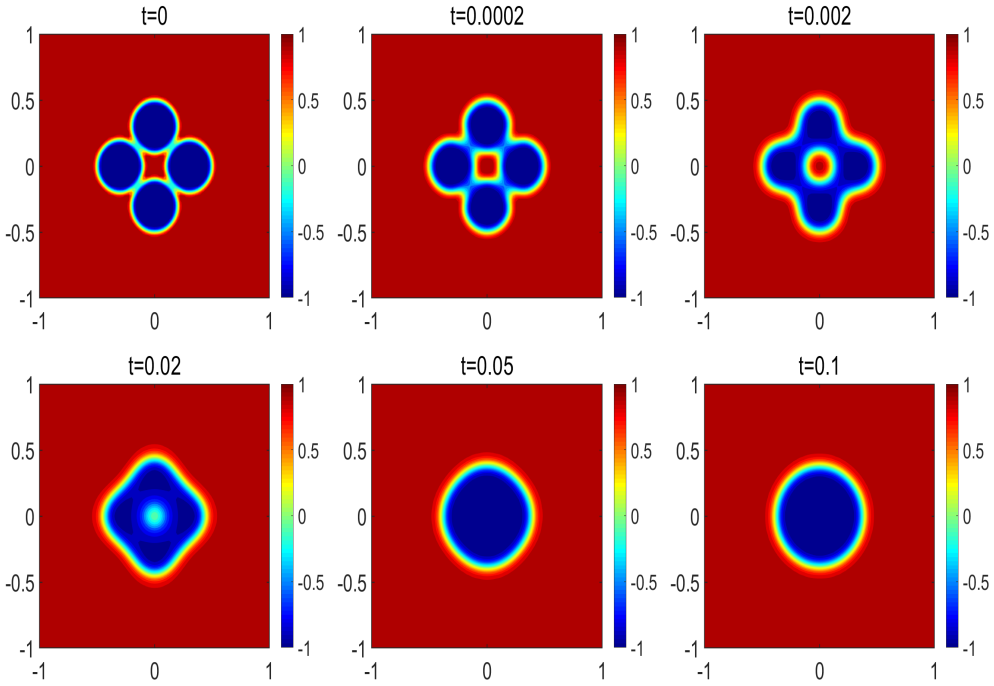

FIGURE 4. **Example 4.3**, P-BDF2 scheme (64)-(65), snapshots of numerical solutions for the phase field function.

A sequence snapshots of the approximate solutions for the phase field function and the velocity field function are produced in Figures 4-5 by the proposed P-BDF2 scheme. It is easy to see the numerical solutions satisfy the expectation. The graphs depicting the evolution of discrete energy and change of total mass for Example 4.3 are presented in Figure 6. As illustrated, the discrete energy decreases over time and the variation in mass approaches machine precision.

Example 4.4. Let domain $\Omega = [-2,2]^2$, define $m_1 = [0,2]$, $m_2 = [0,0]$, $m_3 = [0,-2]$. For given $\epsilon = \frac{1}{16}$, let $r_1 = r_3 = 2 - \frac{3\epsilon}{2}$, $r_2 = 1$ and set $d(x) = \max\{-d_1(x), d_2(x), d_3(x)\}$, $d_j(x) = |x - m_j| - r_j$ for $j = 1,2,3$, we consider

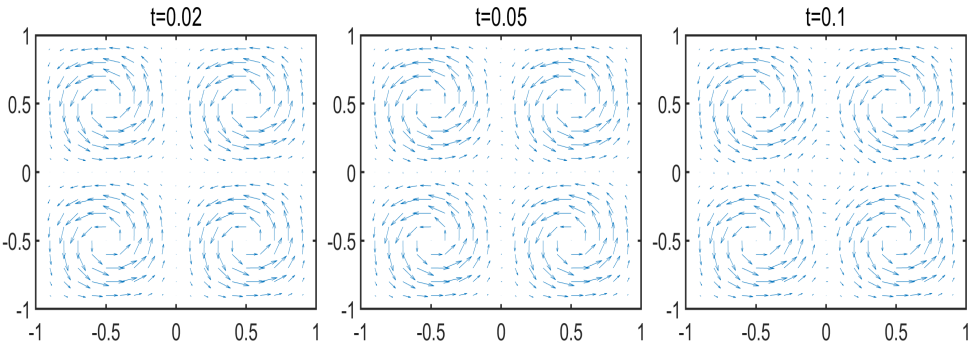

FIGURE 5. **Example 4.3**, P-BDF2 scheme (64)-(65), snapshots of numerical solutions for the velocity field function.

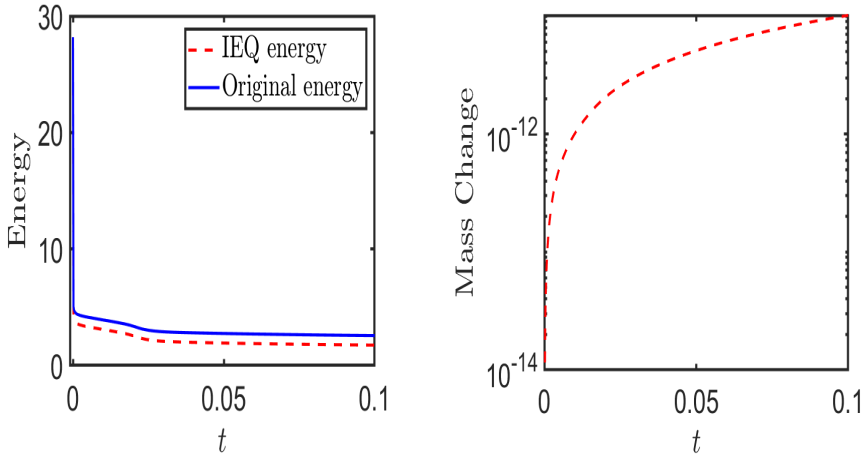

FIGURE 6. **Example 4.3**, the modified discrete energy history and the change of total mass.

the CHNS equations (1) with the following initial condition

$$
\begin{aligned}
&\phi_0 = -\tanh\left(\frac{d(x)}{\sqrt{2}\epsilon}\right), \\
&\mathbf{u}_0 = C\left[\sin(\pi x)^2 \sin(2\pi y) \quad \sin(2\pi x)\sin(\pi y)^2\right]^\top,
\end{aligned} \tag{92}
$$

here the parameters $\mu = \gamma = 1$, $\lambda = \frac{1}{16}$, $C = 100$. We set time step $\tau = 10^{-5}$, the mesh $N \times N = 80 \times 80$, and $B = 1$.

As for the **Example 4.4**, the contour plots of the numerical solutions of ϕ_h^n and $\mathbf{u}_h^n$ by using the P-BDF2 scheme are shown in Figures 7-8. And the evolution of discrete energy and total change of discrete mass are shown in Figure 9. As it is shown, we can also see that the discrete energy decreases over time and the change of total mass reaches machine precision.

Example 4.5. The purpose of this example is to evaluate the long-time performance of the proposed method. Following [9], we consider the CHNS equations (1) with

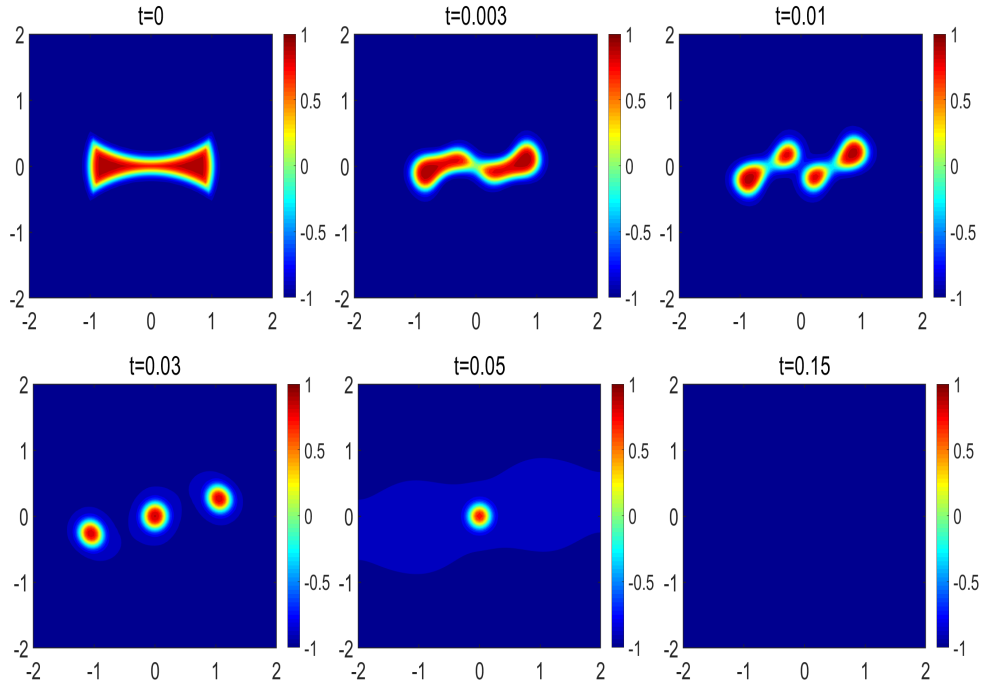

FIGURE 7. **Example 4.4**, P-BDF2 scheme (64)-(65), snapshots of numerical solutions for the phase field function.

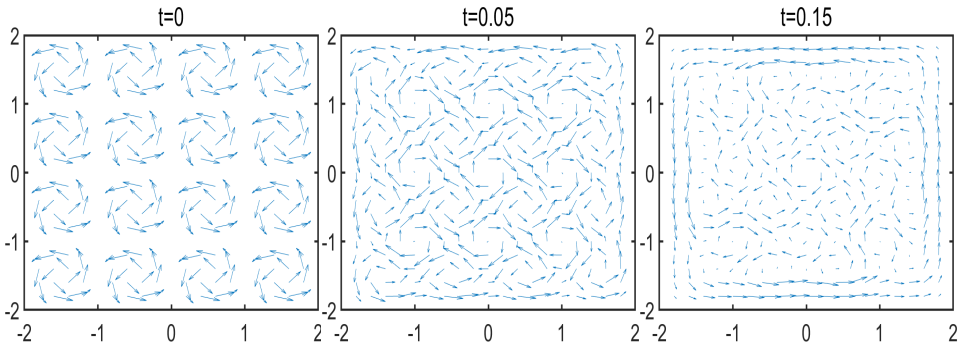

FIGURE 8. **Example 4.4**, P-BDF2 scheme (64)-(65), snapshots of numerical solutions for the velocity field function.

the initial data

$$\begin{aligned} \phi_0 &= 2\text{rand}(x, y) - 1, \\ \mathbf{u}_0 &= \mathbf{0}, \end{aligned} \tag{93}$$

where rand denotes a two-dimensional random function. The parameters are set as $\gamma = 0.002$, $\mu = 1$, $\lambda = 0.01$, $\epsilon = 0.02$. The computational domain $\Omega = [-1, 1] \times [-1, 1]$ is uniformly triangulated using a mesh identified by partition number $N \times N = 160 \times 160$. The final simulation time is $T = 100$ with a time step size $\tau = 10^{-2}$. We solve this problem by the P-BDF1 scheme (24)-(26), with the IEQ auxiliary constant $B = 1$.

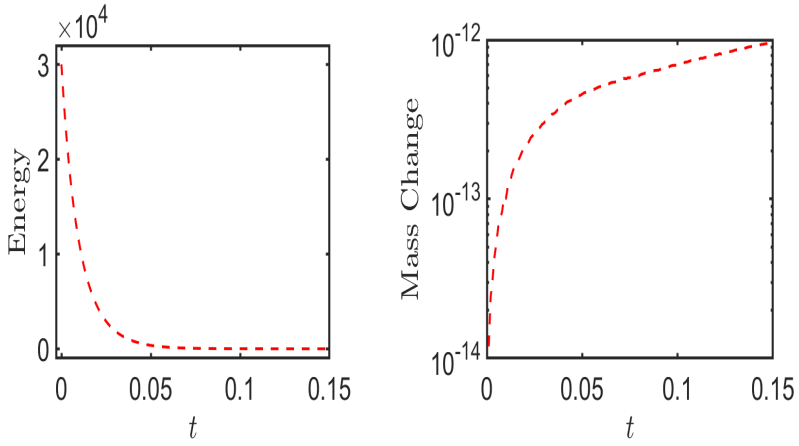

FIGURE 9. **Example 4.4**, the modified discrete energy history and discrete mass variation.

The evolution of the phase function at various times is shown in Figure 10, clearly illustrating the coarsening dynamics. The accompanying plots of energy and mass variations in Figure 11 further confirm that the numerical results preserve the expected physical properties.

Example 4.6. In this example, we demonstrate the flexibility of the proposed method on a curved domain. The same parameters as in **Example 4.5** are used for equation (1), along with the same final simulation time, time-step size, and IEQ auxiliary constant B. The initial condition is given by (93), and the computational domain is defined as $\Omega = (x, y) : x^2 + y^2 \leq 1$. A quasi-uniform triangular mesh with 21,396 nodes is employed for discretization.

Snapshots of the numerical phase function at selected time instances are shown in Figure 12. The energy and mass evolutions are shown in Figure 13, demonstrating both energy dissipation and mass conservation. These results confirm that the proposed scheme performs effectively on curved domains as well.

Example 4.7. [8] Let $\Omega = [-\frac{1}{2}, -\frac{1}{2}] \times [-\frac{1}{5}, -\frac{1}{5}]$, we consider the CHNS equations satisfying the following initial condition

$$\begin{aligned} \phi_0 &= \begin{cases} 1, & x < x_0, \\ -1, & x > x_1, \\ -\sin\left(\dfrac{\pi x}{2x_1}\right), & x_0 \leq x \leq x_1, \end{cases} \\ \mathbf{u}_0 &= [0 \quad 0]^\top, \end{aligned} \tag{94}$$

where $x_1 = x_0 = \frac{\sqrt{2}}{20}$, $\epsilon = \frac{1}{500\sqrt{10}}$, $\lambda = \frac{1}{100}$, $\gamma = \frac{1}{10}$, $\mu = 1$, $\tau = 10^{-7}$, $T = 10^{-5}$.

We solve this problem using the schemes P-BDF1, C-BDF1, and CP-BDF1 with different IEQ constants B, which is introduced in the IEQ approach to ensure $F(\phi_h) + B > 0$. The evolution of the discrete energy of $E\left(\phi_h^{n+1}, \mathbf{u}_h^{n+1}, U_h^{n+1}, p_h^{n+1}\right)$ for P-BDF1 scheme and $E\left(\phi_h^{n+1}, \mathbf{u}_h^{n+1}, U_I^{n+1}, p_h^{n+1}\right)$ for C-BDF1 scheme are shown in Figure 14. From the results, we observe that solutions of the C-BDF1 scheme satisfy the energy dissipation law only when B is sufficiently large, as explained in Remark 3.12, whereas the P-BDF1 scheme satisfies the energy dissipation law

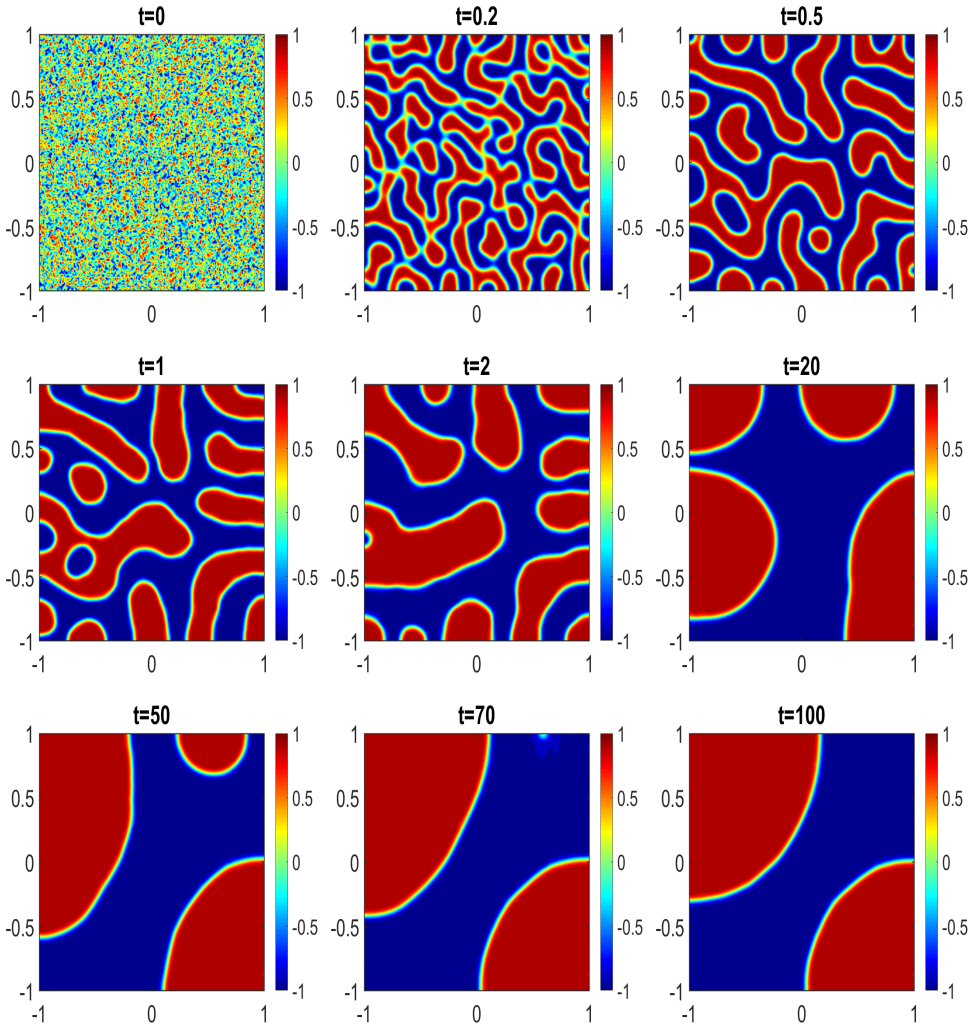

FIGURE 10. **Example 4.5**, P-BDF1 scheme (24)-(26), snapshots of numerical solutions for the phase field function.

regardless of the choice of B. There are noticeable discrepancies between the energy curves produced by the C-BDF1 and P-BDF1 schemes when the mesh size is large ($h = \frac{1}{10}$, as seen in Figure 14). However, these differences decrease as h decreases, as illustrated in Figure 15.

To demonstrate how the CP-BDF1 scheme improves the C-BDF1 scheme in preserving the energy dissipation law, we present energy plots from all three schemes for comparison in Figure 16. To capture the energy increase phenomenon in this specific example, the initial computation is performed on a coarse grid with $h = \frac{1}{10}$. At this stage, we observe a significant discrepancy between the energy curves obtained from the C-BDF1 and P-BDF1 schemes. When the CP-BDF1 scheme is applied for correction, a noticeable energy decrease occurs at $t = 9.6 \times 10^{-6}$. As the grid refined to $h = \frac{1}{160}$, the magnitude of this change diminished. The energy curve produced by the CP-BDF1 scheme is aligned with that of the P-BDF1 scheme. Moreover, the difference between the energy curves from the P-BDF1 scheme on

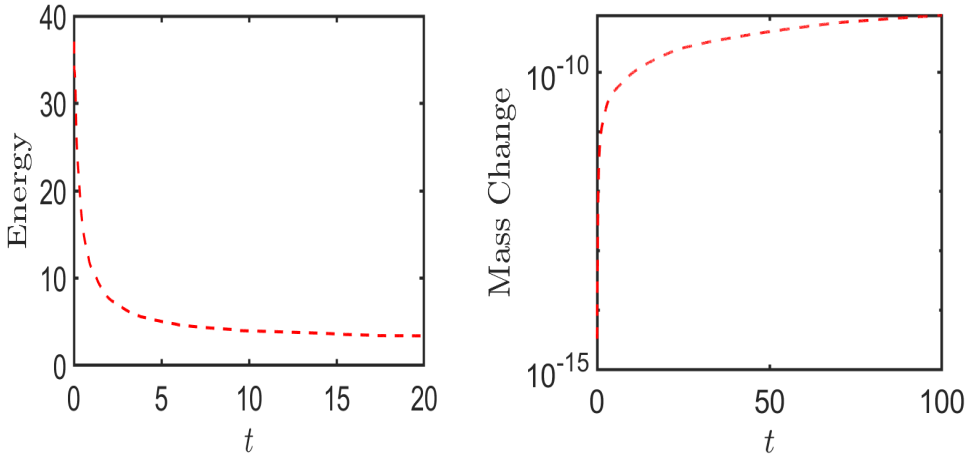

FIGURE 11. **Example 4.5**, the discrete energy history and discrete mass variation.

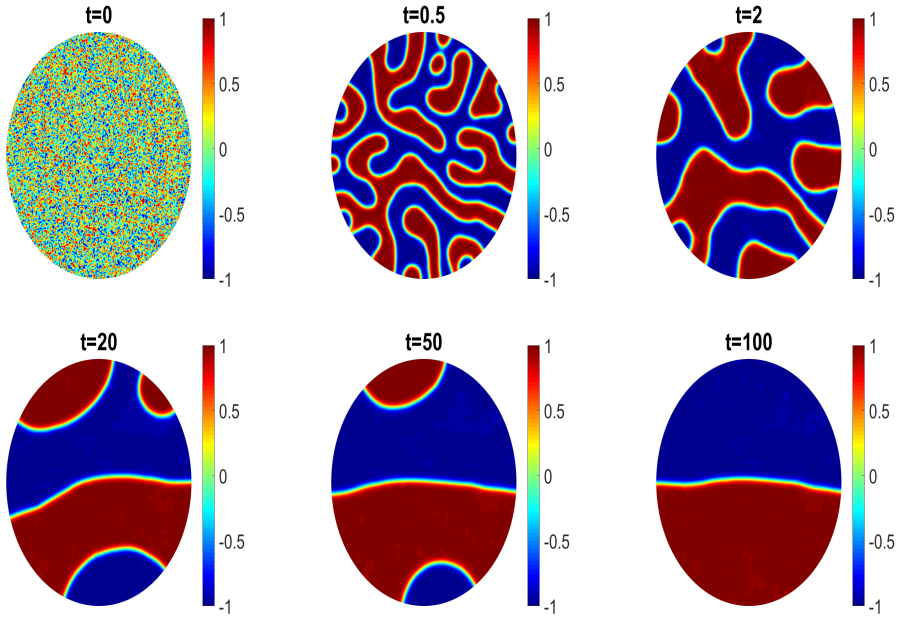

FIGURE 12. **Example 4.6**, P-BDF1 scheme (24)-(26), snapshots of numerical solutions for the phase field function.

coarse and fine meshes is smaller than that of the C-BDF1 scheme. It implies that the modification introduced by the CP-BDF1 scheme is effective in ensuring energy dissipation.

Pictures in the top row of Figure 17 display the phase field plots at $T = 10^{-5}$, computed by using three distinct schemes. slight differences are observed in both the energy curves (Figure 16, left) and the phase field plots (Figure 17, top) on the coarser grid ($h = \frac{1}{10}$). These discrepancies are primarily attributed to the

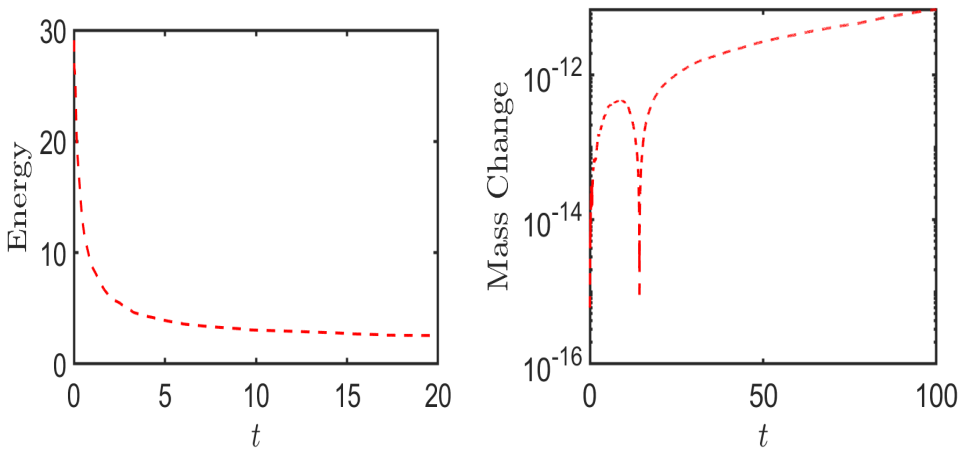

FIGURE 13. **Example 4.6**, the discrete energy history and discrete mass variation.

significant projection error in the intermediate variable U^n. As expected, this error diminishes with increased grid resolution ($h = \frac{1}{160}$; Figure 16, right and Figure 17, bottom), but we can still observe increasing energy for the C-BDF1 scheme. However, the P-BDF1 and CP-BDF1 schemes satisfy the energy dissipation law.

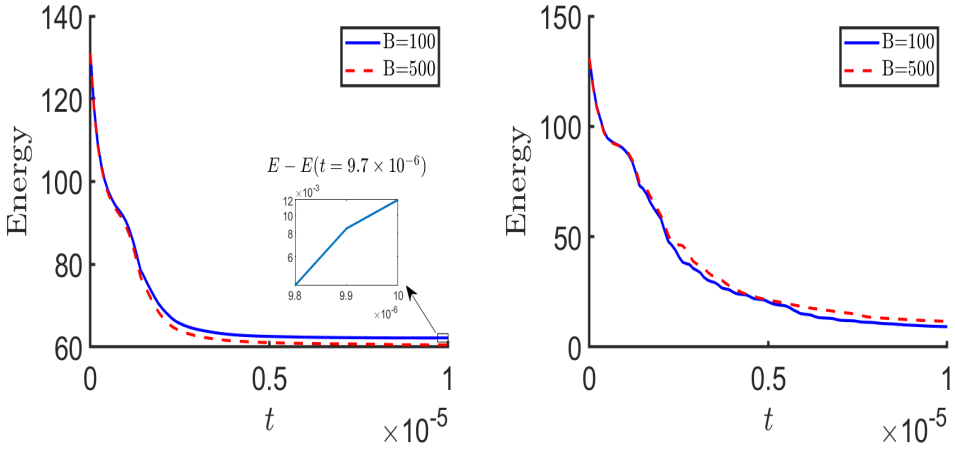

FIGURE 14. **Example 4.7**, Effect of constant B on the discrete energy, Left: C-BDF1 scheme; Right: P-BDF1 scheme, $h = \frac{1}{10}$.

Example 4.8. We design the following three-dimensional test case to assess the capability of the proposed method in handling 3D models. Consider the CHNS equations (1) imposed on the domain $\Omega = [0.2, 0.8] \times [0.2, 0.8] \times [0, 1]$, with initial

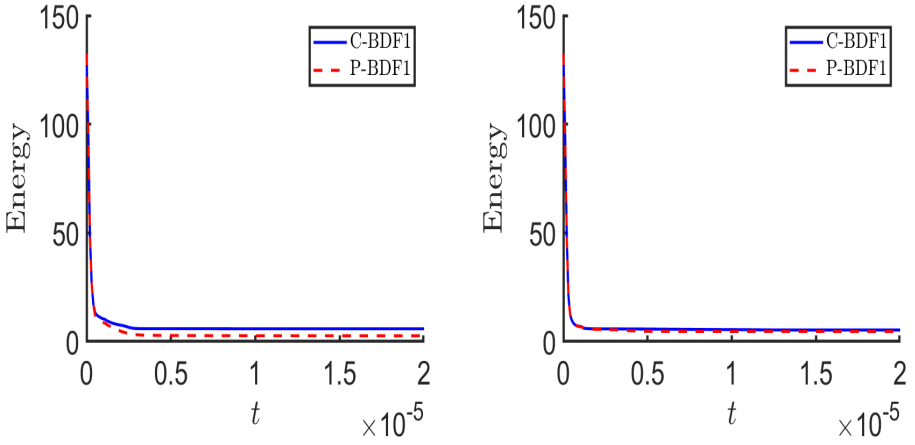

FIGURE 15. **Example 4.7**, Effect of mesh size on the difference of discrete energy, $B = 500$. Left: $h = \frac{1}{160}$; Right: $h = \frac{1}{320}$.

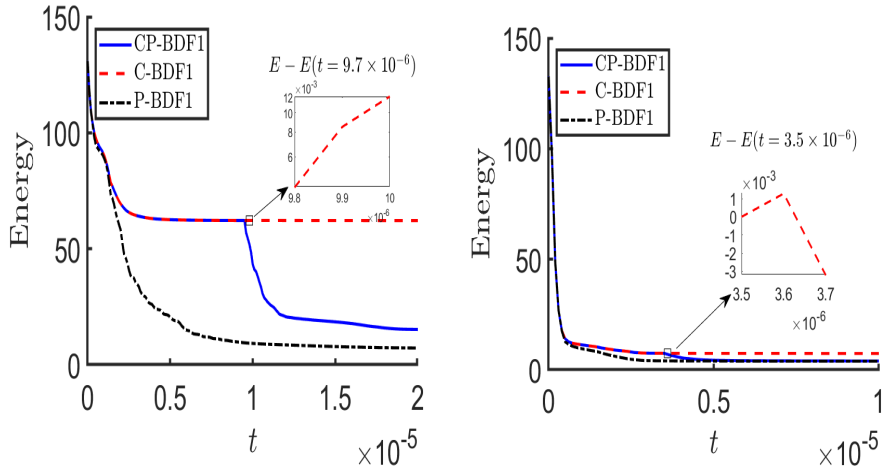

FIGURE 16. **Example 4.7**, The comparison of energy curves for three methods. $B = 100$. Left: $h = \frac{1}{10}$, right: $h = \frac{1}{160}$

conditions specified as

$$\begin{aligned}\phi_0 &= 1 - \tanh\left(\frac{-r + \sqrt{(x-x_a)^2 + (y-y_a)^2 + (z-z_a)^2}}{2\epsilon}\right) \\ &\quad - \tanh\left(\frac{-r + \sqrt{(x-x_b)^2 + (y-y_b)^2 + (z-z_b)^2}}{2\epsilon}\right), \\ \mathbf{u}_0 &= [0,\ 0,\ 0]^\top,\end{aligned} \tag{95}$$

where $x_a = y_a = x_b = y_b = 0.5$, $z_a = 0.65$, $z_b = 0.35$, and $r = 0.15$. Following [28], we choose $\gamma = 0.001$, $\mu = 12$, $\epsilon = 0.02$, $\lambda = 0.05$, and $B = 50$. The problem is solved using the P-BDF1 scheme (24)-(26) with uniform mesh size $h = 1/50$ in all spatial directions and a time step $\tau = 5 \times 10^{-3}$, up to the final time $T = 1$.

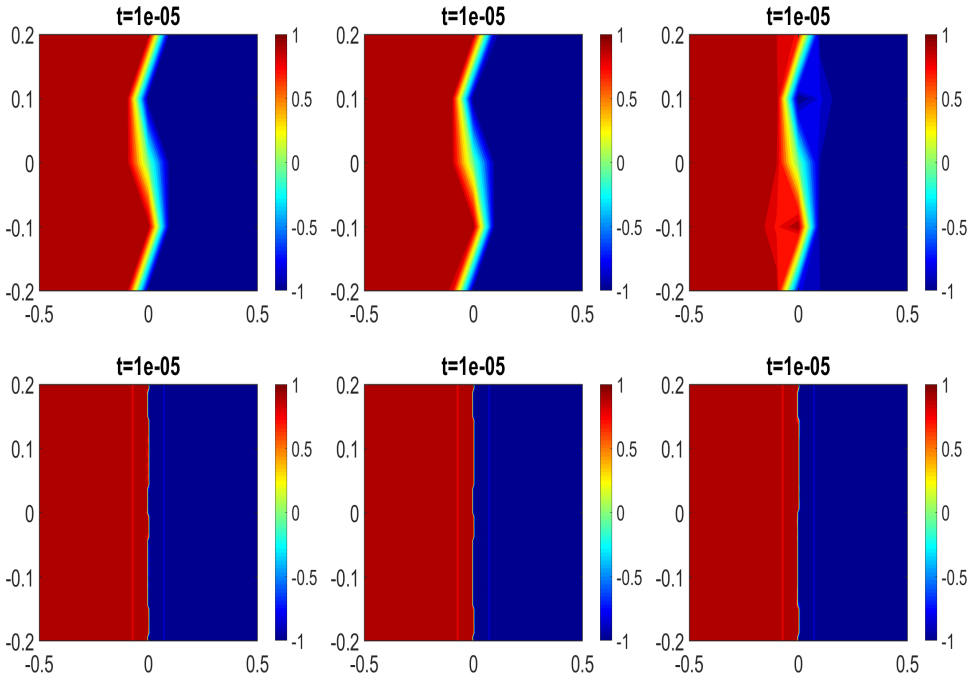

FIGURE 17. **Example 4.7**, The comparison of energy curves for three methods. Top: $h = \frac{1}{10}$, bottom: $h = \frac{1}{160}$; left: CP-BDF1, center: C-BDF1 scheme, right: P-BDF1 scheme.

Figure 18 depicts the coalescence of two interacting bubbles in three dimensions. As time evolves, the bubbles gradually merge into a single, larger bubble driven by surface tension effects, in line with physical expectations [28]. The corresponding energy dissipation and mass variation over time are shown in Figure 19, demonstrating consistency with the theoretical predictions.

5. Conclusion

In this work, we studied three types of first- and second-order IEQ-FEMs for solving the CHNS equations. The first two types position the intermediate function introduced by the IEQ approach either in the continuous function space or in a combination of the continuous function space and finite element space. These methods each exhibit distinct advantages: the former is computationally fast, though the energy may not be fully stable in the FEM space; the latter ensures unconditional energy stability in the FEM space, but the projection step incurs additional computational costs. The third IEQ-FEM scheme is a hybrid of the two, designed to leverage the benefits of both. It begins with the former IEQ-FEM for computational efficiency but switches to the latter if the energy fails to satisfy the energy dissipation property. Numerical examples were presented to validate the theoretical findings and demonstrate the effectiveness of the proposed methods.

A rigorous error analysis for CHNS equations of the proposed methods is desirable and is deferred to future work. Besides, extending the proposed methods to higher-order time discretizations is a potential direction for future research. It would be also interesting in future work to consider deep-learning-type approaches, such as physics-informed neural networks (PINNs) [15, 22].

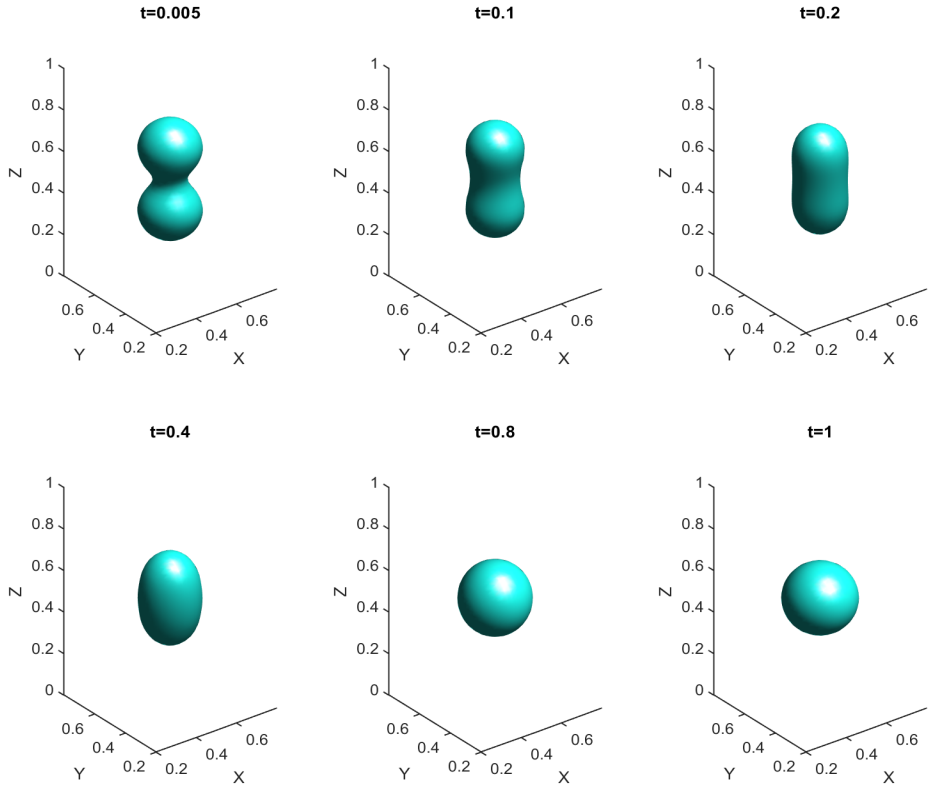

FIGURE 18. **Example 4.8**, P-BDF1 scheme (24)-(26), snapshots of numerical solutions for the phase field function.

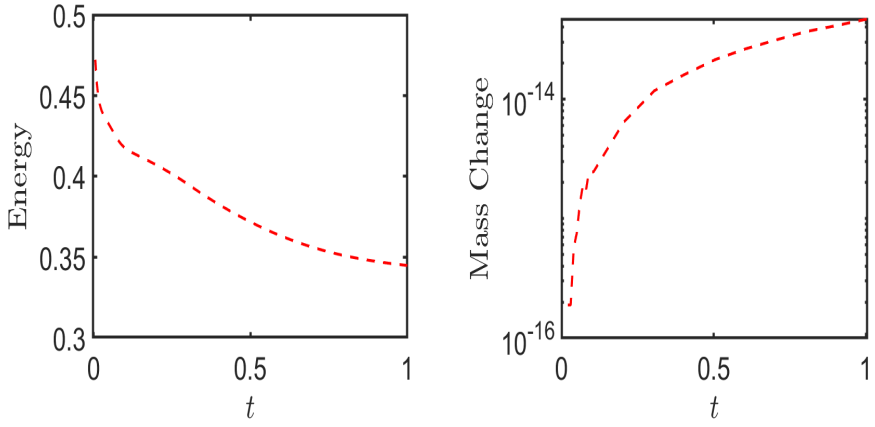

FIGURE 19. **Example 4.8**, the discrete energy history and discrete mass variation.

Acknowledgments

This work was supported by the National Natural Science Foundation of China Project (No. 12571469), Scientific Research Innovation Capability Support Project

for Young Faculty of China (No. SRICSPYF-BS2025132), the Project of Scientific Research Fund of the Hunan Provincial Science and Technology Department (No. 2024JJ1008), the 111 Project (No. D23017), and Program for Science and Technology Innovative Research Team in Higher Educational Institutions of Hunan Province of China.

Author Contributions. Authors are listed in alphabetical order by last name. All authors contribute equally to this manuscript.

Data availability. Not Applicable.

Declarations

Conflict of interests. The authors declare no competing interests.

References

[1] W. Cai, W. Sun, J. Wang, and Z. Yang. Optimal error estimates of unconditionally stable finite element schemes for the Cahn–Hilliard–Navier–Stokes system. *SIAM Journal on Numerical Analysis*, 61(3):1218–1245, 2023.

[2] Y. Cai and J. Shen. Error estimates for a fully discretized scheme to a Cahn-Hilliard phase-field model for two-phase incompressible flows. *Math. Comp.*, 87(313):2057–2090, 2018.

[3] C. Chen and X. Yang. Fully-discrete finite element numerical scheme with decoupling structure and energy stability for the CahnHilliard phase-field model of two-phase incompressible flow system with variable density and viscosity. *ESAIM: M2AN*, 55(5):2323–2347, 2021.

[4] C. Chen and X. Yang. Highly efficient and unconditionally energy stable semi-discrete time-marching numerical scheme for the two-phase incompressible flow phase-field system with variable-density and viscosity. *Sci. China. Math.*, 65(12):2631–2656, 2022.

[5] Y. Chen, Y. Huang, and N. Yi. A decoupled energy stable adaptive finite element method for Cahn-Hilliard-Navier-Stokes equations. *Commun. Comput. Phys.*, 29(4):1186–1212, 2021.

[6] Y. Chen, Y. Huang, and N. Yi. Error analysis of a decoupled, linear and stable Finite Element Method for Cahn-Hilliard-Navier-Stokes equations. *Appl. Math. Comput.*, 421:126928, 2022.

[7] Y. Chen, Y. Huang, N. Yi, and P. Yin. Recovery type a posteriori error estimation of an adaptive finite element method for Cahn–Hilliard equation. *J. Sci. Comput.*, 98(2):35, 2024.

[8] Y. Chen, H. Liu, N. Yi, and P. Yin. Unconditionally energy stable IEQ-FEMs for the Cahn-Hilliard equation and Allen-Cahn equation. *Numer. Algorithms*, 99:1161–1202, 2025.

[9] Y. Chen and J. Shen. Efficient, adaptive energy stable schemes for the incompressible Cahn-Hilliard NavierStokes phase-field models. *J. Comput. Phys.*, 308:40–56, 2016.

[10] J. L. Guermond, P. Minev, and J. Shen. An overview of projection methods for incompressible flows. *Comput. Methods Appl. Mech. Eng.*, 195(44-47):6011–6045, 2006.

[11] J. L. Guermond and L. Quartapelle. On the approximation of the unsteady Navier–Stokes equations by finite element projection methods. *Numerische mathematik*, 80:207–238, 1998.

[12] J.L. Guermond and J. Shen. A new class of truly consistent splitting schemes for incompressible flows. *J. Comput. Phys.*, 192(1):262–276, 2003.

[13] D. Han and X. Wang. A second order in time, uniquely solvable, unconditionally stable numerical scheme for Cahn–Hilliard–Navier–Stokes equation. *J. Comput. Phys.*, 290:139–156, 2015.

[14] M. Hintermller, M. Hinze, and C. Kahle. An adaptive finite element MoreauYosida-based solver for a coupled CahnHilliard/NavierStokes system. *J. Comput. Phys.*, 235:810–827, 2013.

[15] W. Huang, Y. Yang, D. Ammosov, W. Xie, and S. Stepanov. Pinn-based partial learning for multicontinuum problems: Dual continuum fluid filtration simulation. *Advances in Applied Mathematics and Mechanics*, 18(2):537–560, 2026.

[16] Y. Kang, J. Wang, and Y. Yang. Unconditionally energy stable high-order BDF schemes for the molecular beam epitaxial model without slope selection. *Appl. Numer. Math.*, 206:190–209, 2024.

[17] Y. Li and J. Wang. Unconditional convergence analysis of stabilized FEM-SAV method for Cahn-Hilliard equation. *Appl. Math. Comput.*, 419:126880, 2022.

[18] H. Liu and P. Yin. Unconditionally energy stable Discontinuous Galerkin schemes for the Cahn-Hilliard equation. *J. Comput. Appl. Math.*, 390:113375, 2021.

[19] H. Liu and P. Yin. High order unconditionally energy stable RKDG schemes for the SwiftHohenberg equation. *J. Comput. Appl. Math.*, 407:114015, 2022.

[20] J. Lowengrub and L. Truskinovsky. Quasi-incompressible Cahn-Hilliard fluids and topological transitions. *Proc. R. Soc. Lond. A.*, 454(1978):2617–2654, 1998.
[21] H. Ma and P. Huang. Fully discrete schemes with first- and second-order temporal accuracy for the incompressible magnetohydrodynamic flow based on the generalized scalar auxiliary variable approach. *Advances in Applied Mathematics and Mechanics*, 18(1):109–133, 2026.
[22] Maziar Raissi, Paris Perdikaris, and George Em Karniadakis. Physics-informed neural networks: A deep learning framework for solving forward and inverse problems involving nonlinear partial differential equations. *Journal of Computational Physics*, 378:686–707, 2019.
[23] S. Boden S. Aland and et al. Quantitative comparison of Taylor flow simulations based on sharp-interface and diffuse-interface models. *Int. J. Numer. Methods Fluids.*, 73(4):344–361, 2013.
[24] P.A. Nikrityuk S. Eckert and et al. Electromagnetic melt flow control during solidification of metallic alloys. *Eur. Phys. J. Spec. Top.*, 220(1):123–137, 2013.
[25] J. Shen. On error estimates of projection methods for NavierStokes Equations: First-Order schemes. *SIAM J. Numer. Anal.*, 29(1):57–77, 1992.
[26] J. Shen, J. Xu, and J. Yang. A new class of efficient and robust energy stable schemes for gradient flows. *SIAM. Rev. Soc. Ind. Appl. Math.*, 61(3):474–506, 2019.
[27] J. Shen and X. Yang. Energy stable schemes for Cahn-Hilliard phase-field model of two-phase incompressible flows. *Chin. Ann. Math.*, 31(5):743–758, 2010.
[28] Y. Shi, K. Bao, and X. Wang. 3D adaptive finite element method for a phase field model for the moving contact line problems. *Inverse Problems and Imaging*, 7(3):947–959, 2013.
[29] Z. Wang, D. Wang, H. Jia, and C. Zhang. First-order, unconditionally stable, fully decoupled methods for the penalty Ericksen–Leslie system with variable density. *Advances in Applied Mathematics and Mechanics*, 18(2):666–699, 2026.
[30] Z. Xu, X. Yang, and H. Zhang. Error analysis of a decoupled, linear stabilization scheme for the Cahn-Hilliard model of two-phase incompressible flows. *J. Sci. Comput.*, 83(3):57, 2020.
[31] J. Yang, N. Yi, and Y. Chen. Optimal error estimates of a SAV-FEM for the Cahn-Hilliard-Navier-Stokes model. *Comput. Appl. Math.*, 438:115577, 2024.
[32] X. Yang. Linear, and unconditionally energy stable numerical schemes for the phase field model of homopolymer blends. *J. Comput. Phys.*, 302:509–523, 2016.
[33] X. Yang. A new efficient fully-decoupled and second-order time-accurate scheme for Cahn-Hilliard phase-field model of three-phase incompressible flow. *Comput. Methods Appl. Mech. Eng.*, 376:113589, 2021.
[34] X. Yang and H. Yu. Efficient second order unconditionally stable schemes for a phase field moving contact line model using an invariant energy quadratization approach. *SIAM. J. Sci. Comput.*, 40(3):B889–B914, 2018.
[35] X. Yang and G. Zhang. Convergence analysis for the Invariant Energy Quadratization (IEQ) schemes for solving the Cahn-Hilliard and Allen-Cahn equations with general nonlinear potential. *J. Sci. Comput.*, 82(3):55, 2020.
[36] Y. Yang, J. Wang, Y. Chen, and H. Liao. Compatible L2 norm convergence of variable-step L1 scheme for the time-fractional MBE model with slope selection. *J. Comput. Phys.*, 467:111467, 2022.
[37] Z. Yang, L. Lin, and S. Dong. A family of second-order energy-stable schemes for Cahn-Hilliard type equations. *J. Comput. Phys.*, 383:24–54, 2019.
[38] Q. Ye, Z. Ouyang, C. Chen, and X. Yang. Efficient decoupled second-order numerical scheme for the flow-coupled Cahn-Hilliard phase-field model of two-phase flows. *J. Comput. Appl. Math.*, 405:113875, 2022.
[39] P. Yin. *Efficient Discontinuous Galerkin (DG) methods for time-dependent fourth order problems*. PhD thesis, Iowa State University, 2019.
[40] J. Zhao and D. Han. Second-order decoupled energy-stable schemes for Cahn-Hilliard-Navier-Stokes equations. *J. Comput. Phys.*, 443:110536, 2021.
[41] G. Zhu, H. Chen, J. Yao, and S. Sun. Efficient energy-stable schemes for the hydrodynamics coupled phase-field model. *Appl. Math. Model.*, 70:82–108, 2019.
[42] G. Zhu, J. Yao, A. Li, et al. Pore-Scale investigation of Carbon Dioxide-Enhanced oil rRecovery. *Energy Fuels*, 31(5):5324–5332, 2017.

School of Mathematics and Statistics, Anhui Normal University, Wuhu, Anhui 241000, PR China
E-mail: cyy1012xtu@126.com

Hunan Key Laboratory for Computation and Simulation in Science and Engineering, Hunan International Scientific and Technological Innovation Cooperation Base of Computational Science, Xiangtan University, Xiangtan 411105, Hunan, China
E-mail: zuel_ldq@outlook.com

Hunan Research Center of the Basic Discipline Fundamental Algorithmic Theory and Novel Computational Methods, Key Laboratory of Intelligent Computing and Information Processing of Ministry of Education, Xiangtan University, Xiangtan 411105, Hunan, China
E-mail: yangyinxtu@xtu.edu.cn

Department of Mathematical Sciences, The University of Texas at El Paso, El Paso, TX 79968, USA
E-mail: pyin@utep.edu